sustainability

MDPI

Article

Ontology-Driven Semantic Configuration and Prioritization of Earth Observation Opportunities for Sustainable Urban Disaster Response

Jie Li [1], Liang Zhao [2], Bo Jia [3], Xuan Ding [3], Wu Jing [4] and Ke Wang [3,*]

[1] School of Computer Science, China University of Geosciences, Wuhan 430074, China; lijie_gis@cug.edu.cn
[2] Engineering Technology Innovation Center for Ecological Protection and Restoration in the Middle Yellow River, Ministry of Natural Resources, Taiyuan 030024, China; edmend1357@163.com
[3] National Engineering Research Center of Geographic Information System, School of Geography and Information Engineering, China University of Geosciences, Wuhan 430074, China; bo.jia@cug.edu.cn (B.J.); dingxuan@cug.edu.cn (X.D.)
[4] Wuhan Hanyang Municipal Construction Group Co., Ltd., Wuhan 430050, China; m15107194749@163.com
* Correspondence: wangke@cug.edu.cn

Abstract

Sustainable urban disaster response requires Earth observation (EO) resources to be selected according to event demands, environmental conditions, sensing capabilities, and urban targets. This study proposes an Observation Linked Open Data (O-LOD)-based Urban Disaster Observation Task (UDOT) enhancement framework for semantic EO resource configuration. O-LOD organizes heterogeneous data through four dimensions, Event, Context, Subject, and Object, which an instantiation algorithm populates as task graphs. Layered GeoSPARQL queries then match thematic and analytical capabilities, qualify orbit-derived observation opportunities against context and object constraints, and rank feasible alternatives using the Observation Capability Evaluation Model (OCEM). Evaluation on the 2020 Khartoum flood and Bobcat wildfire narrowed 202 satellite–sensor pairs to three flood-capable and four wildfire-capable pairs and returned two Khartoum and eight Bobcat ranked opportunities, with complete queries executing in 3.0 s and 0.07 s. Constraint ablation and resolution sensitivity analyses identified the conditions governing the feasible set. Publicly accessible Sentinel, Landsat, and MODIS products corroborated both retained and excluded results, supporting water-extent and burn-severity mapping where coverage, spectral bands, and image quality met the task requirements. O-LOD therefore provides a traceable semantic link from disaster observation demand to qualified and ranked EO opportunities and subsequent image assessment, supplying task-oriented inputs for downstream scheduling and supporting context-aware sensing for sustainable urban disaster response.

Keywords: geospatial digital twin; intelligent sensing; earth observation task planning; knowledge graph; linked open data; urban disaster response; sustainable urban resilience

Check for updates

Academic Editor: Wen Cheng Liu

Received: 9 July 2026
Revised: 16 August 2026
Accepted: 17 August 2026
Published: 21 August 2026

Copyright: © 2026 by the authors. Licensee MDPI, Basel, Switzerland. This article is an open access article distributed under the terms and conditions of the Creative Commons Attribution (CC BY) license.

1. Introduction

Urban disasters, including floods, storms, landslides, and other climate-related hazards, increasingly threaten the resilience and sustainability of cities [1–4]. Effective disaster monitoring is therefore closely related to sustainable cities and communities, climate adaptation, and resilient infrastructure [5]. Geospatial digital twins have emerged as an important paradigm for representing and managing urban systems by connecting virtual city models

with sensing data and decision-support processes [6–8]. In emergency contexts, however, their operational value depends not only on the fidelity of the virtual representation, but also on whether timely, reliable, and context-appropriate observations can be obtained [9]. Earth observation (EO) resources consequently constitute an essential sensing component of geospatial digital twins for sustainable urban disaster response [10].

Urban disaster monitoring requires high-level information demands to be translated into observation requirements that can be matched with available satellite platforms, sensors, and observation opportunities [11–15]. Resource discovery based on spatial, temporal, and thematic criteria has long been a central goal of the Sensor Web [16,17]. However, disaster-oriented EO resource planning involves more than retrieving existing products or identifying satellites whose nominal footprints cover an area of interest: as urban emergency scenarios become more complex, EO resources must be prospectively configured under changing environmental conditions, limited sensing opportunities, and target-specific observation demands [18,19].

Current EO catalogues, data platforms, and scheduling methods provide important but partial support for this process. The Committee on Earth Observation Satellites (CEOS) and the Observing Systems Capability Analysis and Review Tool (OSCAR) provide rich descriptions of platforms, sensors, and observation capabilities [20,21], but offer limited support for binding these descriptions to dynamic disaster contexts and vulnerable urban targets. Cloud-based platforms such as Google Earth Engine (GEE) and the Hazards Data Distribution System (HDDS) support the discovery and analysis of archived or disaster-related imagery [22,23], but they are not primarily designed to formulate observation demands before acquisition. Satellite scheduling and optimization studies address resource allocation after observation tasks and candidate resources have been defined [24–26]. Although these methods model operational constraints effectively, their task inputs commonly remain limited to predefined time windows, geographic regions, priorities, and resource parameters, with less explicit representation of weather conditions, hazard exposure, urban-object vulnerability, and their semantic relationships [10,27–29].

Ontologies provide a machine-interpretable basis for reducing this semantic gap, but existing models differ substantially in purpose and scope. The Semantic Sensor Network (SSN) ontology and its lightweight Sensors, Observations, Samples, and Actuators (SOSA) core provide general and interoperable descriptions of sensors, observations, samples, procedures, and actuators [30–32], but do not directly define disaster-oriented resource qualification. The Sensor Observation Capability Association (SOCA) ontology and the Observation Capability Association Graph (OCAGraph) represent inherent and dynamic sensor capabilities and their associations [33,34], yet remain primarily capability-centered and provide limited connections to environmental context and vulnerable urban objects. The Flood Process Observation Ontology (OFPO) formalizes flood observation processes and workflows [35], but is designed for a specific hazard domain rather than cross-disaster resource prioritization. The RSISO ontology integrates remote sensing imagery, derived products, and in situ observations [36], while event logic graphs represent event relationships and task dependencies in disaster-chain observation planning [37]. GEOSatDB structures global civil satellite metadata [38], and RSEW-KG organizes multi-source knowledge for remote sensing early warning [39]. These approaches contribute important semantic components, but none provides a unified task-oriented mechanism for linking disaster events, environmental conditions, sensing opportunities, sensor capabilities, and urban observation targets during resource qualification and prioritization.

Linked Open Data (LOD) and geospatial knowledge graphs provide the integration foundation required for such a mechanism [40]. KnowWhereGraph and GeoGraphVis demonstrate how heterogeneous environmental, geographic, and disaster information can

be connected for knowledge discovery and decision support [41,42]. GeoSPARQL and related geospatial linked-data technologies further enable spatial representation, querying, and reasoning over Resource Description Framework (RDF) graphs [43–46]. Nevertheless, most geospatial knowledge graphs are used primarily for data integration, exploratory querying, visualization, or retrospective analysis. The remaining limitation is not simply the availability of spatial predicates such as containment and intersection, but the absence of task semantics that explain why a spatial relation, contextual condition, or sensing capability is relevant to a particular observation demand. Consequently, current approaches remain limited in answering which EO resources can observe which urban targets, during which opportunities, under which environmental conditions, and with what traceable supporting evidence.

This limitation is particularly consequential for geospatial digital twins and intelligent sensing. A digital twin for urban disaster response should not only represent changes in urban space but also support the sensing actions required to update, inspect, and reason about those changes [9,10], and it is precisely this task-oriented semantic layer that existing digital-twin studies, EO catalogues, sensor ontologies, and geospatial knowledge graphs leave unspecified [6–8,40–46].

To address this need, an Observation Linked Open Data (O-LOD)-based Urban Disaster Observation Task (UDOT) enhancement framework is developed. Grounded in DOLCE + DnS Ultralite (DUL) [47], O-LOD organizes EO task knowledge into four interacting dimensions: ObservationEvent, ObservationContext, ObservationSubject, and ObservationObject. A boundary model and an instantiation algorithm transform heterogeneous open and domain data into an RDF-based semantic configuration space, in which intrinsic resource requirements and cross-dimensional *event–context–subject–object* constraints are evaluated through GeoSPARQL queries. Feasible resources are then prioritized using an ontology-embedded scoring function adapted from the Observation Capability Evaluation Model (OCEM) [48], extending the workflow from binary candidate pruning to capability-based ranking. The contribution is twofold: O-LOD provides a unified and traceable representation of disaster events, environmental conditions, sensing capabilities, and vulnerable urban targets, and the enhanced UDOT workflow supports prospective resource configuration, prioritized candidate selection, and post-event EO data discovery. The framework is assessed on two contrasting cases, the 2020 Khartoum flood and the 2020 Bobcat wildfire, using constraint-ablation experiments, query and graph-construction measurements, and archived EO imagery to examine the effects of the four semantic dimensions, computational performance, candidate ranking, and the usability of the selected resources relative to excluded or lower-ranked alternatives.

The remainder of this paper is organized as follows. Section 2 presents the proposed UDOT enhancement framework. Section 3 describes the two case studies and reports the experimental results. Section 4 discusses the implications, comparative assessment, and sustainability relevance of the framework. Section 5 concludes the paper and outlines future research directions.

2. UDOT Enhancement Framework

2.1. Framework Components

Figure 1 presents the overall architecture of the proposed framework, which translates disaster-oriented observation needs into semantically explicit EO resource plans. Through O-LOD, the framework connects urban disaster events, environmental context, urban observation targets, and EO sensing resources so that observation requirements can be evaluated through RDF graph patterns, temporal conditions, and GeoSPARQL spatial predicates. The workflow consists of five phases:

- Urban Disaster Event (Trigger): An identified urban disaster event triggers observation requirements and defines the task's spatiotemporal and thematic scope.
- O-LOD Harvesting: Heterogeneous open and domain datasets describing the event, environmental and socioeconomic context, urban objects, EO platforms, and sensors are collected and qualified according to the O-LOD boundary model.
- O-LOD Instantiation: Qualified data are transformed into RDF triples and organized as a semantically interlinked knowledge graph. This phase establishes the semantic configuration space for UDOT formulation.
- UDOT Configuration: Fine-grained observation intents are translated into dimension-specific and cross-dimensional constraints. These constraints jointly express event requirements, environmental conditions, target characteristics, and the availability and capabilities of EO resources. Constrained evaluation returns EO resources and observation opportunities satisfying the declared constraints, together with the evidence supporting their qualification. When several feasible alternatives remain, an OCEM-based score prioritizes them.
- Observation Response: The ranked, evidence-linked resource plan supports subsequent mission scheduling or image acquisition for disaster-oriented analysis.

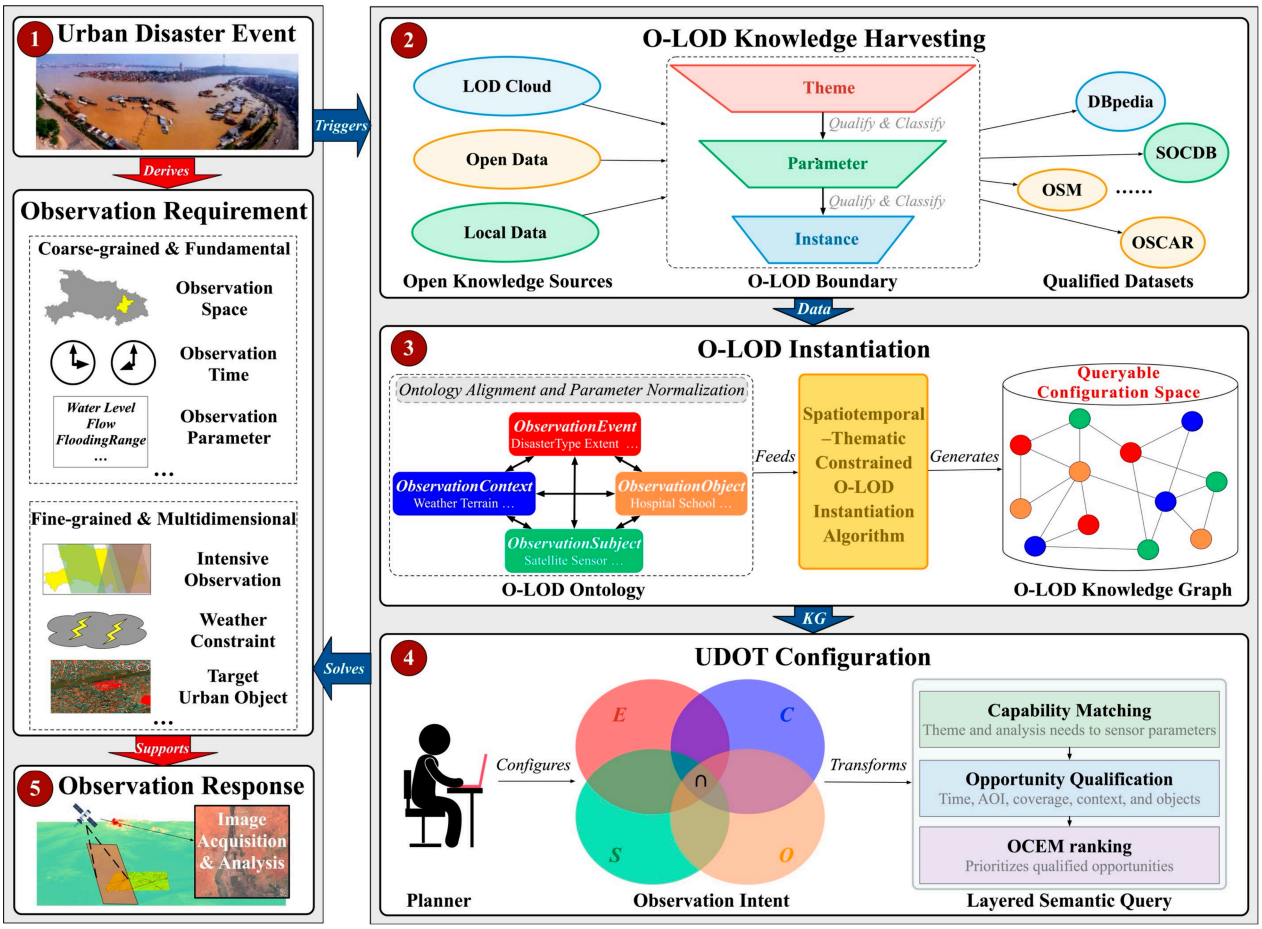


Figure 1. Overview of the UDOT enhancement framework.

2.2. O-LOD Conceptual Design

2.2.1. Design Rationale and Scope

Urban disaster response requires EO resources to be configured not only according to where and when an event occurs, but also according to the environmental conditions, urban-object characteristics, and available sensing capabilities. Therefore, O-LOD organizes

the UDOT knowledge space around four mutually constrained semantic dimensions: ObservationEvent (*E*), ObservationContext (*C*), ObservationSubject (*S*), and ObservationObject (*O*). Formally, this O-LOD knowledge space is represented as $K = <E, C, S, O>$. The event defines the disaster-driven observation demand; the *context* captures environmental and socioeconomic conditions that affect observation feasibility and priority; the subject describes EO platforms, their predicted opportunities, and the sensors that can perform observation; and the object represents urban entities whose exposure, criticality, or monitoring need motivates sensing.

Figure 2 illustrates how O-LOD transforms conventional observation requirements into a semantically enriched configuration space for fine-grained observation task configuration. Observation requirements are conventionally expressed as coarse specifications in a Spatial–Temporal–Thematic space, $R(S_p, T_m, Th)$. O-LOD expands this representation into $K = \langle E, C, S, O \rangle$, in which each dimension retains spatial, temporal, and thematic characteristics while performing a distinct semantic role. Together, the entities and relations in these four dimensions constitute the semantic configuration space in which multidimensional UDOTs are formulated.

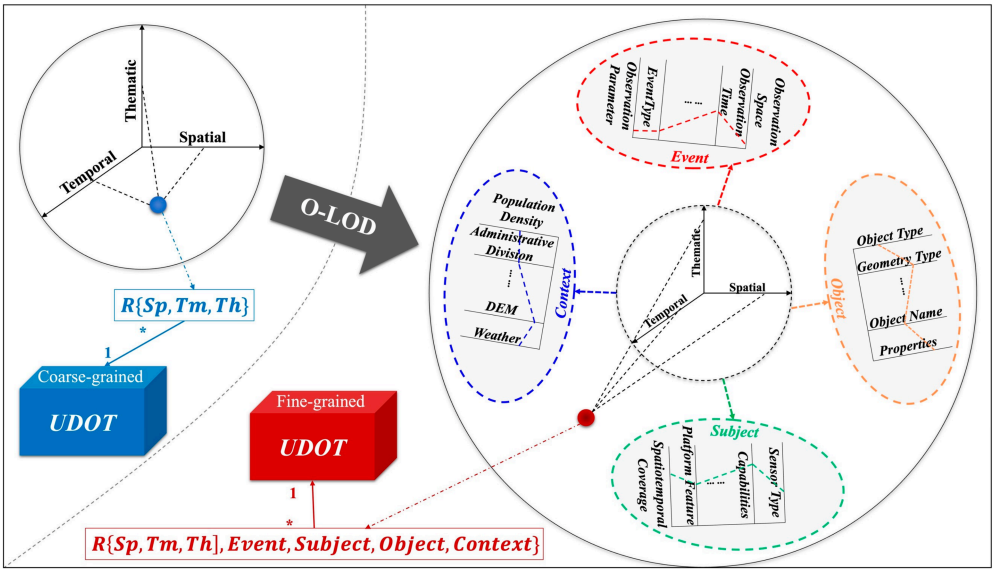


Figure 2. Conceptual refinement of a UDOT from Spatial–Temporal–Thematic requirements to the four-dimensional O-LOD configuration space (1 and * indicate one-to-many cardinality).

2.2.2. O-LOD Boundary

Figure 3 presents the radial and hierarchical architecture of the O-LOD boundary model, which defines how candidate open spatiotemporal datasets are qualified and classified before entering the knowledge graph. The model defines three levels that progressively refine the granularity of knowledge organization:

- Theme: Represents the four core dimensions of O-LOD. A harvested dataset must contribute task-relevant evidence to at least one dimension in *K*.
- Parameter: Represents a controlled data or knowledge category within a theme. For example, remote sensing satellites constitute a parameter category of EO resources within the Subject dimension.
- Instance: Represents a concrete entity within a category. For example, Fengyun-3D can be represented as an instance of a remote sensing satellite.

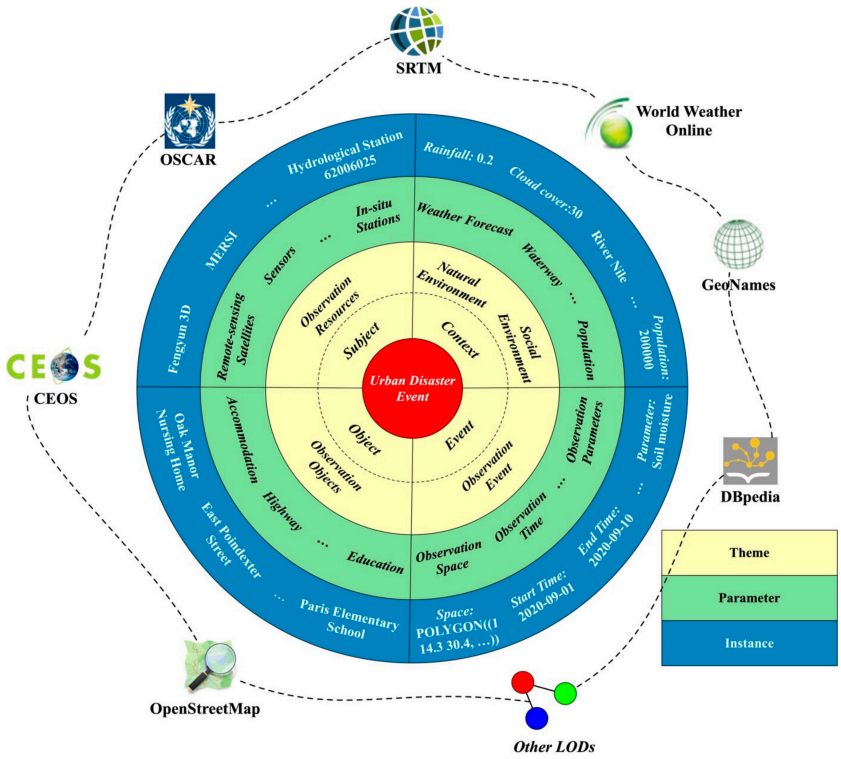


Figure 3. Architecture and an illustrative instantiation of the O-LOD boundary model.

The outermost layer represents candidate multisource datasets eligible for O-LOD construction. It first tests each source for task relevance and then assigns qualified content to an appropriate parameter category. For example, hourly records retrieved from the World Weather Online API are qualified under ObservationContext and classified as dynamic meteorological evidence, from which precipitation, cloud cover, and wind attributes can be instantiated. At the parameter level, semantically equivalent fields from heterogeneous sources are mapped to shared categories before their instances are created. This organization keeps the graph focused on task-relevant evidence while preserving a common structure across data sources.

2.3. O-LOD Ontology Design

The boundary model determines which data may enter the graph, whereas the ontology specifies how disaster-oriented observation knowledge is organized and related. As shown in Figure 4, the ontology comprises four modules aligned with the dimensions of the conceptual model and with relevant DUL categories [48]. Their cross-module relations form a demand–context–resource–target structure: an ObservationEvent o_lod:requiresObservation from an ObservationSubject and o_lod:existsIn an ObservationContext; the ObservationContext o_lod:contains relevant ObservationObjects and o_lod:influences the suitability of an ObservationSubject; and the ObservationSubject o_lod:observes the target object and o_lod:providesObservation for the ObservationEvent.

The ontology adopts two complementary levels of relations. The high-level properties above express the conceptual interactions among the four modules, whereas module-specific properties describe event time and space, environmental elements, platform–sensor associations, sensing capabilities, spatiotemporal availability, and object features. This organization preserves the overall semantics of the observation task while providing the detailed paths required for RDF and GeoSPARQL queries. The principal relations used to interpret Figures 4–8 are summarized in Table 1.

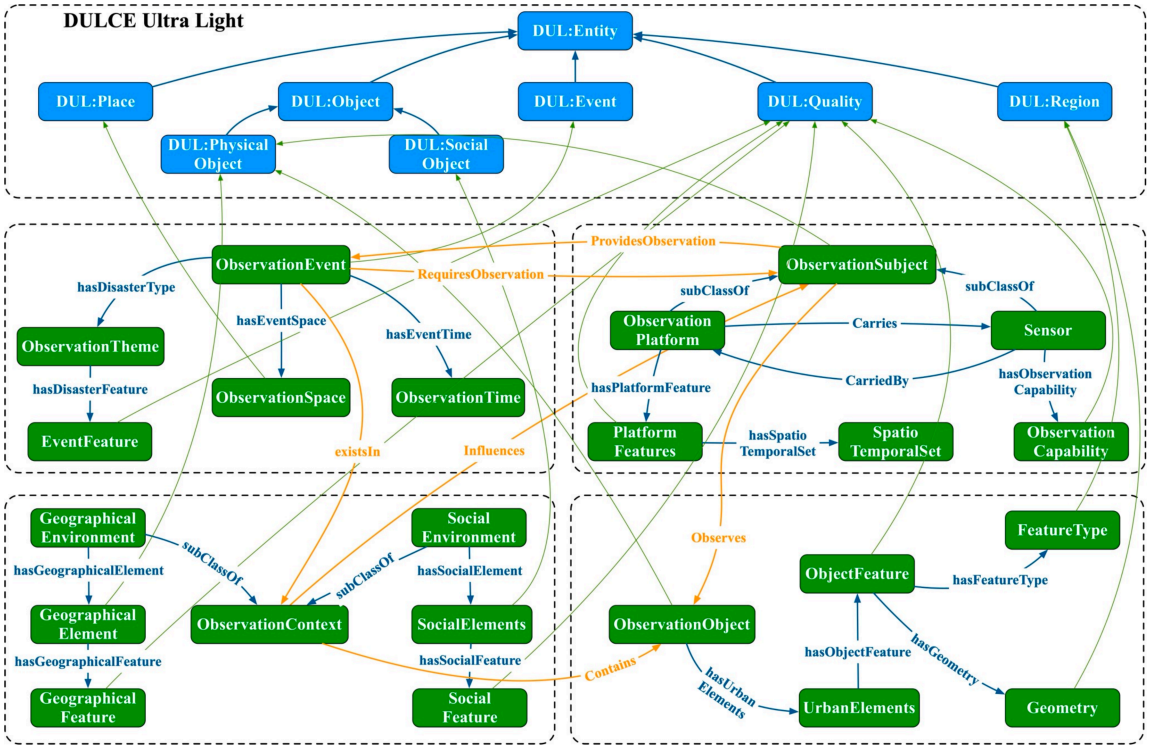


Figure 4. The O-LOD ontology modules, core classes, and relations aligned with DUL.

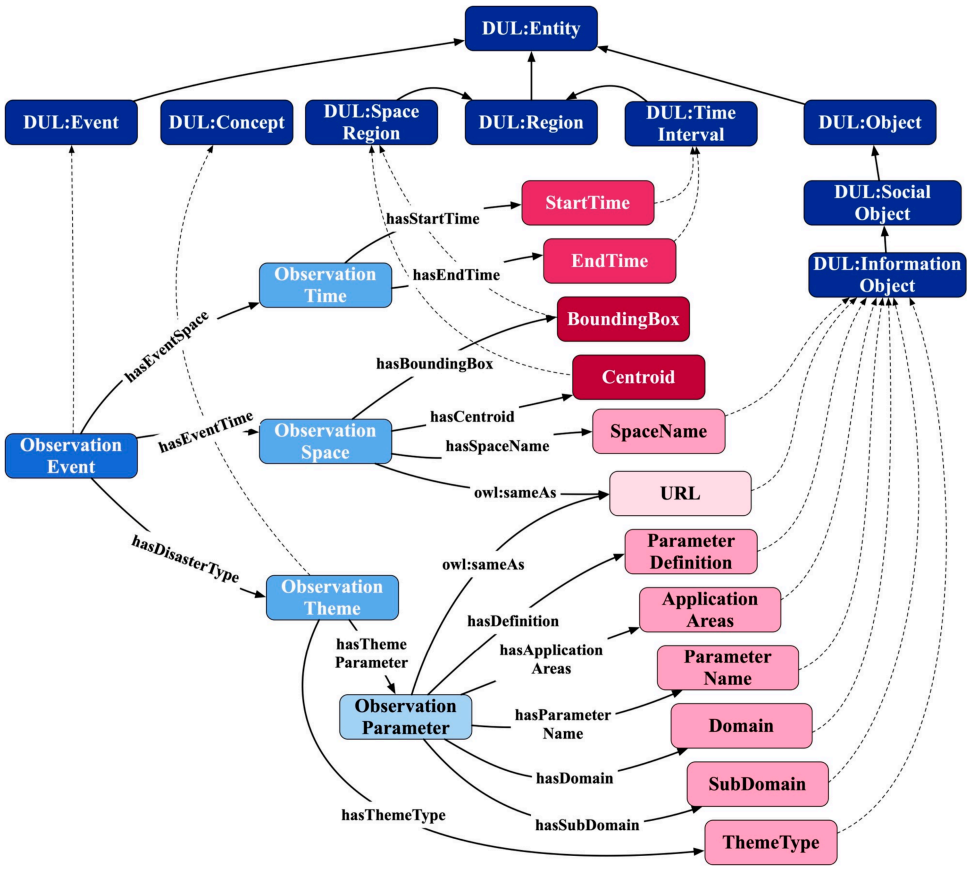


Figure 5. Core classes of the ObservationEvent module.

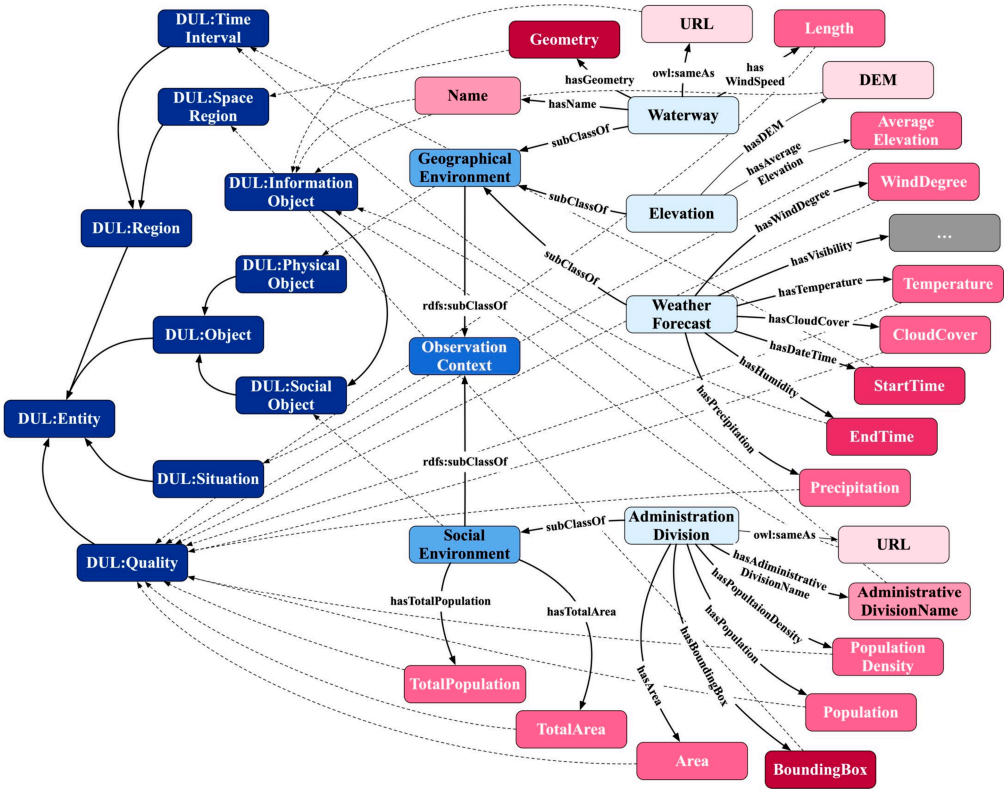


Figure 6. Core classes of the ObservationContext module.

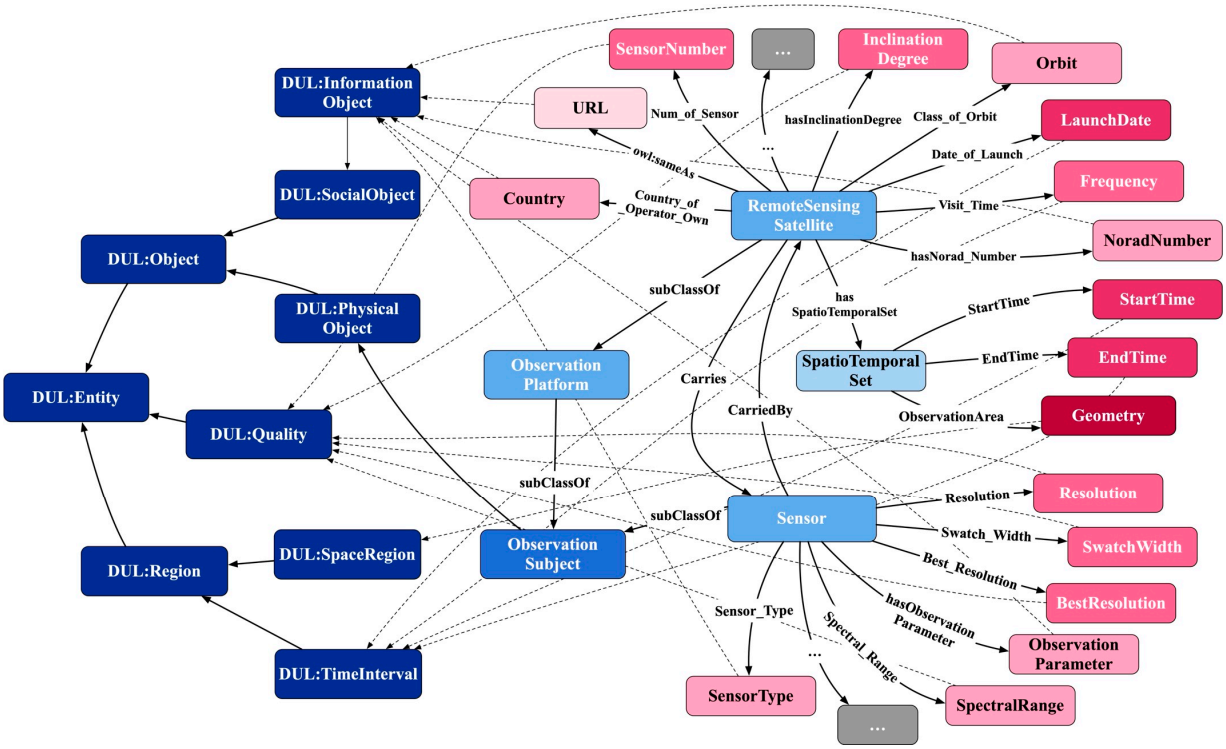


Figure 7. Core classes of the ObservationSubject module.

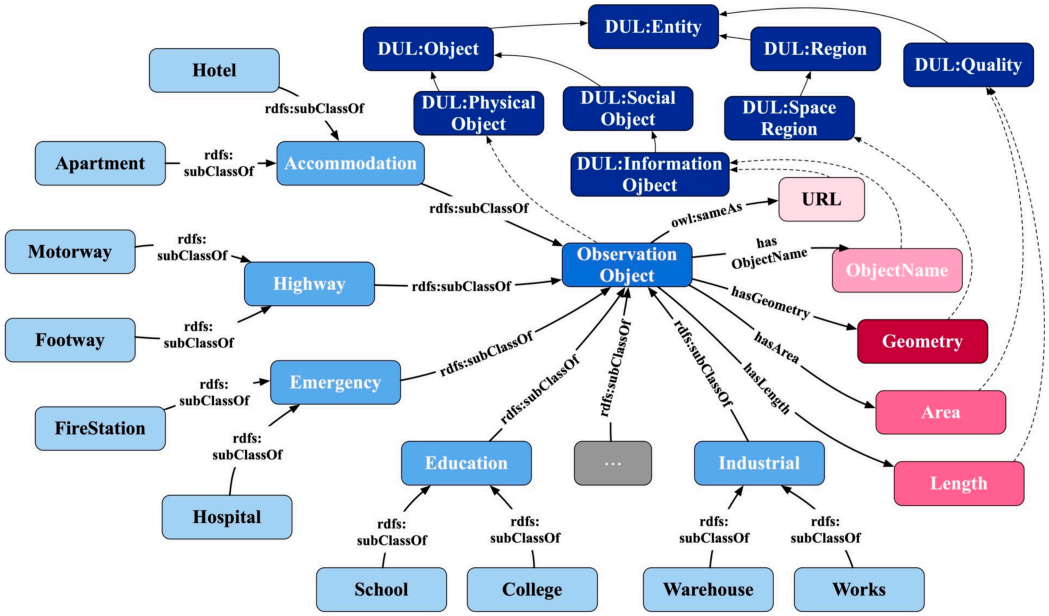


Figure 8. Core classes of the ObservationObject module.

Table 1. Core O-LOD relation glossary.

Relation	Domain	Range	Semantic Definition
o_lod:requiresObservation	ObservationEvent	ObservationSubject	Expresses an event-driven demand for an EO subject capable of providing the required observation.
o_lod:providesObservation	ObservationSubject	ObservationEvent	Expresses the observation response that a subject can provide for an event.
o_lod:existsIn	ObservationEvent	ObservationContext	Associates an event with the geographical and socioeconomic context in which the observation demand arises.
o_lod:influences	ObservationContext	ObservationSubject	Indicates that contextual conditions affect the suitability or priority of an EO subject.
o_lod:contains	ObservationContext	ObservationObject	Associates a context with the urban objects relevant to the observation task.
o_lod:observes	ObservationSubject	ObservationObject	Relates an EO subject to the physical target of observation.
o_lod:hasEventTime/o_lod:hasObservationTime	ObservationEvent	ObservationTime	Links an event to the temporal interval of its observation demand.
o_lod:hasEventSpace/o_lod:hasObservationSpace	ObservationEvent	ObservationSpace	Links an event to its geographical extent.
o_lod:hasDisasterType/o_lod:hasObservationTheme	ObservationEvent	ObservationTheme	Links an event to its disaster-oriented observation theme.
o_lod:hasObservationParameter	ObservationTheme; Sensor	ObservationParameter	Relates thematic requirements or sensor capabilities to a controlled observation parameter.
o_lod:Carries	ObservationPlatform	Sensor	Relates an EO platform to an onboard sensor.
o_lod:hasSpatioTemporalSet	ObservationPlatform	SpatioTemporalSet	Describes the spatial coverage and temporal availability of an EO platform.
o_lod:hasGeometry/geo:asWKT	Spatial entity	Geometry/geo:wktLiteral	Provides the geometry used to evaluate spatial relations.

2.3.1. ObservationEvent Module

The ObservationEvent module formalizes the disaster occurrence that initiates an observation demand (Figure 5). An ObservationEvent is characterized by an ObservationTheme, an ObservationTime τ_{evt}, and an ObservationSpace B_{evt}. The ObservationTheme describes the disaster type and associated observation parameters, the ObservationTime

defines the interval over which the demand is active, and the ObservationSpace specifies the affected or task-relevant geographical extent. These elements provide a common event reference for connecting contextual conditions, target objects, and EO resources.

2.3.2. ObservationContext Module

The ObservationContext module represents the environmental and human-system conditions in which an observation task is formulated (Figure 6). It comprises GeographicalEnvironment and SocialEnvironment. GeographicalEnvironment describes physical and dynamic conditions such as terrain, elevation, hydrography, hazard extent, and weather, whereas SocialEnvironment describes administrative, demographic, and other socioeconomic characteristics. Contextual elements may be spatially and temporally qualified, allowing the ontology to represent both relatively stable background conditions and dynamic conditions that influence the feasibility or priority of EO resources.

2.3.3. ObservationSubject Module

The ObservationSubject module represents the EO resources capable of performing observations (Figure 7). It distinguishes an ObservationPlatform from the sensors carried by that platform. The platform is associated with its spatial coverage and temporal availability through a SpatioTemporalSet, whereas each Sensor is associated with ObservationCapabilities describing the phenomena or parameters it can observe and its relevant sensing characteristics, enabling an observation requirement to be matched to an EO platform–sensor combination.

2.3.4. ObservationObject Module

The ObservationObject module represents the physical urban targets that motivate an observation task (Figure 8). It classifies objects into functional categories such as accommodation, transportation, healthcare, education, emergency facilities, communication infrastructure, and industrial facilities. Each object may be described by geometry, type, source identifier, and task-relevant attributes.

Urban vulnerability is represented through combinations of object-related indicators rather than a universal binary attribute. Such indicators may describe hazard exposure, structural susceptibility, functional criticality, population or service dependence, accessibility, land use, and observed damage or deformation. This structure is consistent with multivariate remote-sensing-based infrastructure vulnerability assessment [49,50] and allows different disaster-oriented tasks to select and combine the indicators relevant to their target objects. The ontology thus provides a semantic structure for object characterization without prescribing a single vulnerability model for all hazards.

2.4. Semantic Formulation of UDOTs

2.4.1. O-LOD Instantiation

The Spatiotemporal–Thematic Constrained Instantiation Algorithm constructs the instance graph $G_{inst} = (V, A)$ from heterogeneous object, context, and EO-resource sources (Algorithm 1). Its input event is represented as $E_{trigger} = < Type, \tau_{evt}, B_{evt} >$, where τ_{evt} and B_{evt} denote the event interval and geographical extent. The functions F_{sp}, F_{tm}, and F_{th} test spatial, temporal, and thematic relevance, respectively. Source records that satisfy the applicable constraints are mapped to O-LOD classes and properties; their geometries and times are represented in forms suitable for GeoSPARQL and temporal comparison.

Algorithm 1: Spatiotemporal–thematic constrained instantiation algorithm.

Input: $E_{trigger}$: Disaster trigger event $< Type,\ \tau_{evt}, B_{evt} >$; $D_{obj},\ D_{ctx},\ D_{sub}$: Heterogeneous object, context, and EO-resource data sources; K_{O_LOD}: O-LOD ontology
Output: $G_{inst} = (V, A)$: Instantiated O-LOD knowledge graph

Initialize G_{inst} with $v_e \longleftarrow InstantiateEvent(E_{trigger}, K_{O_LOD})$
$\Theta_{evt} \leftarrow ThemeParameters(Type, K_{O_LOD})$; Attach$(v_e,\ \tau_{evt}, B_{evt}, \Theta_{evt})$
//Phase 1: Spatial-Thematic Object Instantiation
$O_{raw} \leftarrow Query\left(D_{obj}\right)$
for each $x \in O_{raw}$:
    if $F_{sp}(x, B_{evt}) \wedge F_{th}(x, \Theta_{evt})$ **then**
        $v_o \leftarrow Instantiate(x, K_{O_LOD}.Object)$; AddEdge$(v_e, v_o)$
//Phase 2: Spatiotemporal Context Instantiation
$C_{raw} \longleftarrow Query(D_{ctx})$
for each $x \in C_{raw}$:
    if $F_{sp}(x, B_{evt}) \wedge F_{tm}(x, \tau_{evt})$ **then**
        $v_c \leftarrow Instantiate(x, K_{O_LOD}.Context)$; AddEdge$(v_e, v_c)$
//Phase 3: Spatiotemporal Subject Instantiation
$P_{raw} \leftarrow Query(D_{sub})$
for each $p \in P_{raw}$
    $Q_p \leftarrow CarriedSensors(p)$
    $A_p \leftarrow \{a \in SpatioTemporalSets(p, Q_p, \tau_{evt}) | F_{sp}(a, B_{evt}) \wedge F_{tm}(a, \tau_{evt})\}$
    $v_s \longleftarrow$ InstantiateResource$(p, Q_p, A_p, K_{O_LOD}.Subject)$; AddEdge$(v_s, v_e)$
$G_{inst} \longleftarrow linkDimensions(G_{inst}, K_{O_LOD})$
Return G_{inst}

The algorithm first instantiates the event and resolves its thematic parameters. Its three phases then instantiate spatially and thematically relevant urban objects, spatiotemporally relevant contextual records, and EO resource subgraphs. For each platform, Q_p denotes its carried sensors and A_p denotes the platform-owned spatiotemporal sets satisfying the event area and interval. InstantiateResource creates platform, sensor, and spatiotemporal set instances together with the o_lod:Carries and o_lod:hasSpatioTemporalSet relations. Sensor capability and platform availability remain connected through their common platform node. The resulting instances are connected according to the inter-module relations defined in Section 2.3. Stable Internationalized Resource Identifiers (IRIs) are assigned in accordance with Linked Data vocabulary-use principles [51], forming the configuration space on which UDOT constraints are evaluated.

2.4.2. UDOT Configuration

Following the construction of G_{inst}, UDOT configuration maps an observation intent to constraints over the four O-LOD dimensions. In the virtual scenario shown in Figure 9, ObservationEvent specifies the task area and interval; ObservationSubject supplies an optical sensing resource, its observation parameter, and spatiotemporal availability; ObservationContext provides weather and terrain conditions; and ObservationObject identifies the target type, geometry, and elevation. Temporal and spatial relations connect these elements into a jointly qualified opportunity set.

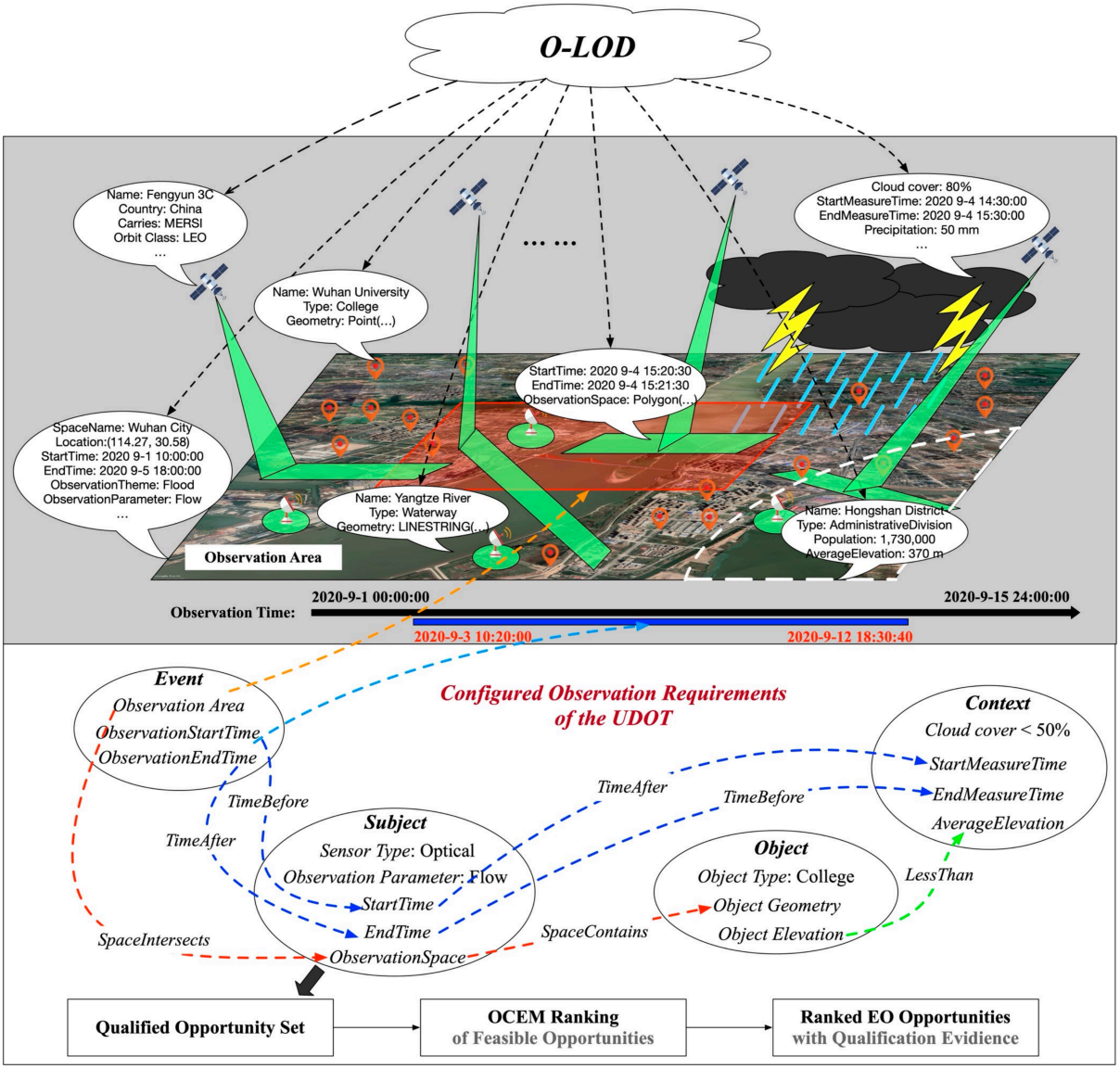


Figure 9. Virtual scenario illustrating multidimensional UDOT qualification and the subsequent OCEM ranking of feasible EO opportunities.

Let E, C, S, and O denote the sets of *event*, *context*, *subject*, and *object* instances in G_{inst}. For a particular UDOT, $e \in E$ is the trigger event, $c \in C$ is the relevant contextual evidence, $o \in O$ is a target object or target set, and $s \in S$ denotes an EO subject associated with a specific spatiotemporal set. The qualified subject set is

$$S^* = \{s \in S | C_{attr}(s, o, c, e) \wedge C_{ent}(s, o, c, e)\}, \tag{1}$$

where C_{attr} and C_{ent} denote dimension-specific and cross-dimensional constraints, respectively. Dimension-specific constraints evaluate attributes within each O-LOD dimension:

$$C_{attr}(s, o, c, e) = C_E^{scope}(e) \wedge C_C^{value}(c) \wedge C_S^{cap}(s) \wedge C_O^{type}(o), \tag{2}$$

where C_E^{scope} checks the completeness of the event specification, C_C^{value} evaluates declared contextual thresholds, C_S^{cap} tests the requested observation parameters and sensing capabilities, and C_O^{type} tests the target category and intrinsic object attributes.

Cross-dimensional constraints require graph paths connecting two or more dimensions:

$$C_{ent}(s,o,c,e) = C_{ES}^{time}(e,s) \wedge C_{ES}^{space}(e,s) \wedge C_{CS}^{time}(c,s) \wedge C_{CO}^{trelation}(c,o) \wedge C_{SO}^{fitness}(s,o). \quad (3)$$

Here, C_{ES}^{time} and C_{ES}^{space} compare a subject's availability with the event interval and area; C_{CS}^{time} associates that availability with context valid at the same time; $C_{CO}^{relation}$ evaluates the target against its environmental or socioeconomic context; and $C_{SO}^{fitness}$ tests whether the sensing resource is suitable for the target scale and observation purpose. Consequently, a subject that satisfies a capability requirement within the Subject dimension is retained only when its availability also satisfies the relevant Event, Context, and Object relations shown in Figure 9. The constraints can be translated into a coupled GeoSPARQL graph pattern. Table 2 gives a compact fragment corresponding to Figure 9; prefix declarations and selected literal attributes are omitted for readability.

Table 2. Multidimensional GeoSPARQL query corresponding to the UDOT in Figure 9.

```
PREFIX o_lod: <http://bigdatasensing.cn/o_lod/>
PREFIX geof:  <http://www.opengis.net/def/function/geosparql/>
PREFIX uom:   <http://www.opengis.net/def/uom/OGC/1.0/>
PREFIX xsd:   <http://www.w3.org/2001/XMLSchema#>
SELECT DISTINCT ?satellite ?sensor ?opportunity ?object
WHERE { ?event a  o_lod:ObservationEvent ;
    o_lod:hasObservationTime ?eventTime ;
    o_lod:hasObservationSpace/o_lod:BoundingBox ?eventArea ;
    o_lod:hasObservationTheme/o_lod:hasObservationParameter ?requiredParameter .
  ?eventTime o_lod:StartTime ?taskStart ; o_lod:EndTime ?taskEnd .
  ?satellite a o_lod:satellite ; o_lod:Carries ?sensor ;
    o_lod:hasSpatioTemporalSet ?opportunity .
  ?sensor o_lod:Sensor_Type ?sensorType ;
    o_lod:hasObservationParameter ?requiredParameter .
  ?opportunity o_lod:StartTime ?passStart ; o_lod:EndTime ?passEnd ;
    o_lod:Geometry ?footprint .
  ?context a o_lod:GeographicalEnvironment ;
    o_lod:hasWeatherCondition ?weather ; o_lod:hasWaterway ?river ;
    o_lod:hasElevation/o_lod:AverageElevation ?meanElevation .
  ?weather o_lod:StartMeasureTime ?weatherStart ;
    o_lod:EndMeasureTime ?weatherEnd ; o_lod:Cloudcover ?cloud .
  ?river o_lod:Geometry ?riverGeometry .
  ?object a o_lod:college ; o_lod:Geometry ?objectGeometry .
  BIND(geof:buffer(?riverGeometry, 1000, uom:metre) AS ?riverBuffer)
  BIND(o_lod:dem_value(?objectGeometry) AS ?objectElevation)
  FILTER(LCASE(STR(?sensorType)) = "optical")
  FILTER(?taskStart <= ?passStart && ?passEnd <= ?taskEnd &&
         ?weatherStart <= ?passStart && ?passEnd <= ?weatherEnd && xsd:double(?cloud) < 50)
  FILTER(geof:sfIntersects(?eventArea, ?footprint) &&
         geof:sfContains(?footprint, ?objectGeometry) &&
         geof:sfIntersects(?riverBuffer, ?objectGeometry))
  FILTER(?objectElevation < ?meanElevation)
}
```

The shared ObservationParameter resource aligns event demand with sensor capability, GeoSPARQL property paths compress multi-hop navigation, and RDF Schema (RDFS) subclass entailment allows subclasses of ObservationObject to satisfy a general target requirement, and the opportunity and context paths bind the temporal and spatial predicates to explicit graph entities. GeoSPARQL therefore evaluates the spatial relations, while O-LOD provides the typed cross-dimensional paths and evidence bindings through which those relations acquire task-specific meaning.

If $|S^*| > 1$, the qualified alternatives are subsequently ordered using an adaption of OCEM. For normalized decisive factors x_d, weighted factors x_i, weights w_i, and scaling coefficient α, the score is

$$OCEM(s) = \left[\prod_{d \in D} \exp(1 + \alpha x_d)\right] \exp\left(1 + \alpha \frac{\sum_{i \epsilon W} w_i x_i}{\sum_{i \epsilon W} w_i}\right). \quad (4)$$

The factors summarize the coverage, thematic, environmental, temporal, revisit, resolution, and spectral or radiometric characteristics of the qualified resources. OCEM is used only to prioritize the members of S^*; it does not alter the multidimensional qualification model defined in Equations (1)–(3).

3. Experiments and Results

The proposed framework was evaluated using two urban disaster cases: the 2020 Khartoum flood and the 2020 Bobcat wildfire. For each case, multisource data describing the event, observation context, EO resources, and urban objects were instantiated as an O-LOD knowledge graph and queried to discover, qualify, and rank observation opportunities. Archived EO products were subsequently retrieved to verify representative selected and excluded results.

3.1. Study Areas and Open Data Sources

3.1.1. Study Areas

Khartoum, the capital of Sudan, lies near the confluence of the White and Blue Niles and contains dense urban infrastructure within a low-relief, flood-prone environment (Figure 10a). In September 2020, severe flooding affected much of Sudan, with Khartoum State among the most affected areas. The study area spans 32.3426–32.7215° E and 15.3696–15.7343° N, and the task window extends from 5 September 2020 06:00 to 10 September 2020 18:00. Its combination of riverine flood exposure, urban infrastructure, terrain variation, and changing weather provides a representative setting for flood-oriented EO resource planning. The Bobcat Fire occurred in the Angeles National Forest, California, and began on 6 September 2020 in the mountainous area surrounding Mount Wilson (Figure 10b). The study area spans 118.07–118.02° W and 34.20–34.25° N, and the task window extends from 6 September to 1 October 2020. Its combination of rapidly changing fire conditions, rugged terrain, nearby critical infrastructure, and variable atmospheric conditions provides a contrasting setting for wildfire-oriented EO resource planning.

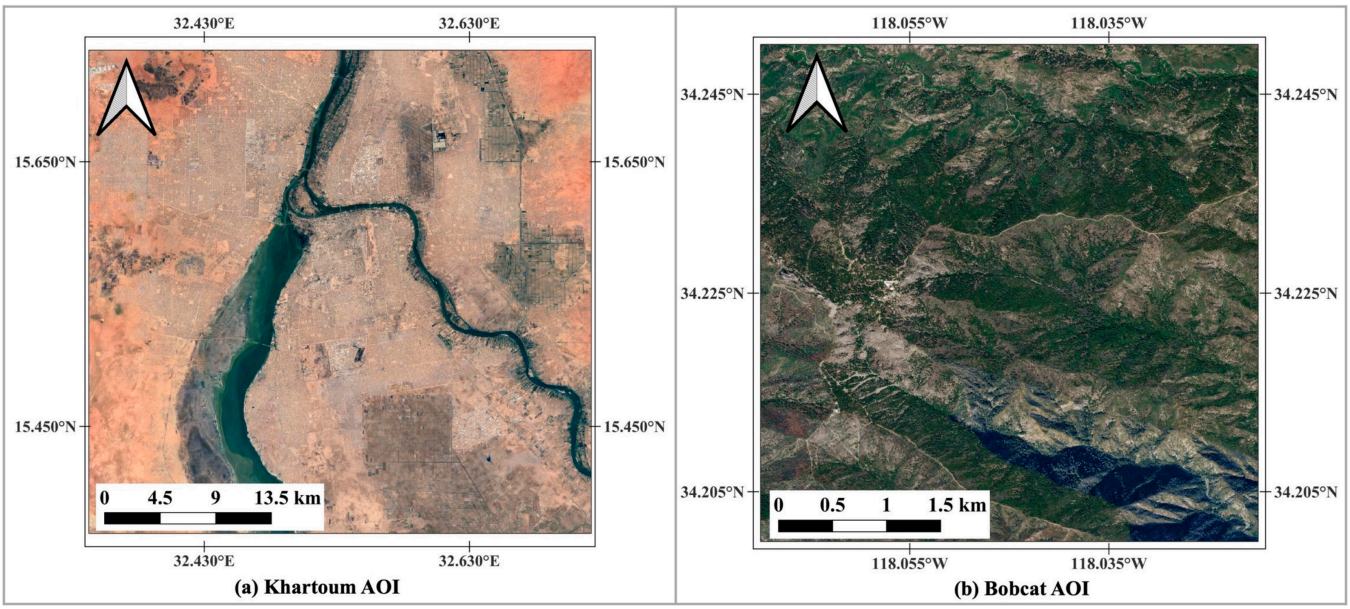


Figure 10. Boundaries of the two study areas.

3.1.2. Open Data Sources

Table 3 summarizes the data used to instantiate the two case graphs and evaluate the resulting resource-planning decisions, covering linked place and urban-feature records,

hourly atmospheric and terrain information, two-line element sets (TLEs), platform and sensor-capability descriptions, and the historical Bobcat perimeter.

Table 3. Overview of selected data sources.

Source	Type	Graph Dimension or Function	Data Used
DBpedia, GeoNames	LOD	Event/Object	External identifiers and general place information
OpenStreetMap	LOD	Context/Object	Khartoum waterways and roads; Bobcat roads, facilities, power, and communication objects
World Weather Online	OD	Context	Historical hourly modeled weather linked to opportunity intervals
AWS Terrain Tiles/SRTM	OD	Context	Numeric DEMs for Khartoum and Mount Wilson terrain queries
Space-Track/CelesTrak	OD	Subject	Historical TLEs and NORAD identifiers for SGP4 opportunity generation
CEOS, OSCAR, UCS	OD	Subject	Platform, sensor, observation-parameter, and capability facts
SOCDB	LD	Subject	Curated local sensor-capability facts and normalized parameter mappings
NIFC/USFS perimeter	OD	Event/Context	Historical Bobcat Fire perimeter and target-distance evidence
Public STAC catalogues	OD	Archive discovery and validation	Sentinel, Landsat, and MODIS product identifiers, footprints, bands, and scene quality

LOD: Linked Open Data; OD: Open Data; LD: Local Data.

Public SpatioTemporal Asset Catalog (STAC) services [52] were used as external archive-discovery interfaces rather than as an O-LOD semantic dimension. The qualified opportunities were associated with archive records to examine product coverage, scene cloud, readable bands, and image-derived monitoring evidence. Observation time and provenance were retained so that contextual information and product-level measurements remained distinguishable in the graph.

3.2. Cross-Case O-LOD Knowledge Graph Instantiation

The source records listed in Table 3 were harvested and transformed by the O-LOD instantiation algorithm described in Section 2.4.1. Historical TLEs identified through satellite NORAD numbers were propagated with sensor swath widths to instantiate satellite-owned hasSpatioTemporalSet nodes; each node records its sensor, time interval, and well-known text (WKT) footprint. Hourly weather records were represented as weather conditions of the geographical environment through the existing hasWeatherCondition relation and were matched to opportunity intervals by temporal conditions in the task queries. Source identifiers and provenance links were retained for externally derived entities, and the resulting RDF datasets were loaded into GraphDB (Ontotext, Sofia, Bulgaria) [53] for GeoSPARQL evaluation.

The Khartoum experiment used the approximately 566,000-statement base graph together with named graphs containing TLE- and swath-derived observation opportunities (22,510 statements), hourly weather records (4957 statements), and normalized sensor capabilities (2647 statements). Complete orbit and swath inputs were available for 143 satellites. Of the 202 satellite–sensor pairs described in the capability graph, 173 pairs on 96 satellites produced 1023 intersections with the area of interest (AOI). The 144 hourly weather records provided the temporal context evaluated for these opportunities, and the capability graph supplied normalized resolution and swath values together with 306 explicit spectral-band descriptions.

For the Bobcat case, the same algorithm generated a 25,013-statement task graph from the historical fire perimeter, 600 hourly weather records, SRTM terrain data, 1955 OpenStreetMap (OSM)-derived urban objects, and the shared EO-resource graph. It reuses 136 satellite and 104 sensor IRIs and contains 15 predicted observation opportunities, of which eight satisfy the task constraints.

Graph construction and query execution were performed on an Apple M3 Max computer (Apple Inc., Cupertino, CA, USA) with 14 CPU cores and 36 GB memory, using GraphDB 10.8.4, RDF4J 4.3.15, and Java 21.0.6. During query timing, the full GraphDB repository contained 883,358 explicit and inferred statements across the default graph and the experiment-specific named graphs. Separately, instantiation of the 25,013-statement Bobcat task graph from prepared source records averaged 3.544 $\pm$ 0.329 s over five runs.

Figure 11 presents a simplified view of representative Khartoum instances within the four ontology modules. It shows how the disaster event is connected to its observation theme, time, and space; how terrain and social information form the observation context; and how EO platforms, spatiotemporal sets, and urban objects retain links to CEOS, OSCAR, GeoNames, DBpedia, OSM, and the source geospatial datasets.

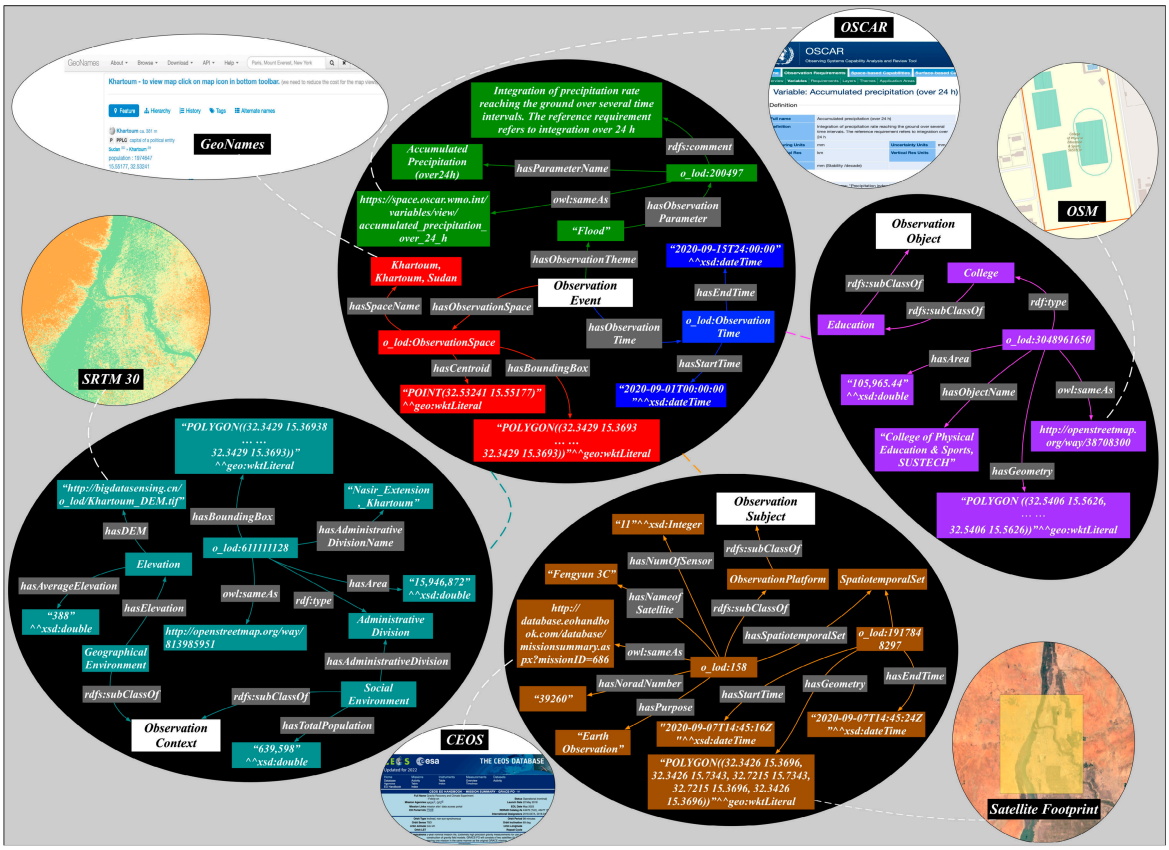


Figure 11. Composition and representative semantic links of the instantiated knowledge graph.

3.3. Formulation of UDOTs

Disaster observations become operationally useful when the detected hazard can be related to urban elements whose accessibility or function may be affected. In Khartoum, monitoring surface-water expansion along the Blue Nile and its relation to nearby roads can indicate where flood conditions may disrupt urban access. In the Bobcat case, characterizing burn severity around Mount Wilson can support the prioritization of post-fire inspection for critical and surrounding infrastructure. These two monitoring needs were formulated as the UDOT configurations in Table 4.

Table 4. Monitoring needs and ontology-aligned configurations of the two UDOTs.

O_LOD Dimension	Role	Khartoum Flood	Bobcat Wildfire
Observation Event	Monitoring objective and theme Event AOI and observation window	Detect surface-water expansion along the Blue Nile and relate it to roads that may affect urban accessibility Khartoum AOI; 5–10 September 2020	Characterize burn severity around Mount Wilson and relate it to critical and surrounding infrastructure Mount Wilson AOI; 6 September–1 October 2020
Observation Context	Acquisition conditions Hazard and terrain setting	Hourly cloud cover $\leq 50\%$ Blue Nile 2 km corridor and contextual mean elevation of 388 m.	Hourly cloud cover $\leq 50\%$ Historical fire perimeter and contextual mean elevation of 1365.05 m
Observation Subject	Thematic and analytical capability Observation opportunity	Flood-theme parameter match; Green and SWIR1 bands; resolution ≤ 30 m TLE-derived opportunity within the observation window; AOI coverage ≥ 0.8; solar elevation $> 0^\circ$	All four wildfire-theme parameters; NIR and SWIR2 bands; resolution ≤ 30 m. TLE-derived opportunity within the task window; AOI coverage ≥ 0.8; solar elevation $\geq 10^\circ$
Observation Object	Urban target and hazard relation	Residential roads within the river corridor with mean DEM elevation below the contextual average	Mount Wilson and surrounding infrastructure; the target is within 100 m of the fire perimeter and above the contextual mean elevation

Several task conditions are parameterized from the ObservationContext dimension rather than fixed globally. The minimum solar elevation is one such parameter: over the low-relief Khartoum plain, water delineation is insensitive to illumination geometry, so any daylight acquisition is admissible ($\geq 0^\circ$), whereas over the rugged Mount Wilson terrain low sun angles introduce cast shadow and slope–aspect illumination differences that propagate into dNBR, so a stricter minimum ($\geq 10^\circ$) is imposed.

3.4. UDOT Query Execution and Results

3.4.1. Layered Construction of UDOT Queries

The UDOT queries were constructed and executed in two layers. The first layer retrieved satellite–sensor pairs and their observation opportunities together with the values required to test the task conditions. It did not calculate an OCEM score, allowing each condition to be removed in turn and the query to be re-executed for the ablation analysis. The second layer applied all conditions simultaneously and ranked the qualified opportunities with OCEM. The principal GeoSPARQL constructions in the two layers are summarized in Table 5.

Table 5. Layered construction and experimental roles of the UDOT queries (Ellipses indicate omitted arguments or query patterns).

Layer	Query Component	Representative GeoSPARQL Construction	Role
First	Event and subject	?event o_lod:hasObservationSpace/o_lod:BoundingBox ?eventArea; o_lod:hasObservationTheme ?theme. ?satellite o_lod:Carries ?sensor.	Retrieves resource pairs and tests theme, band, and resolution requirements.
	Observation opportunity	?satellite o_lod:hasSpatioTemporalSet ?opportunity. ?opportunity o_lod:StartTime ?start; o_lod:EndTime ?end; o_lod:Geometry ?footprint.	Binds the acquisition time, footprint, predicted coverage, and solar elevation.
	Context and object	?opportunity o_lod:hasModeledWeatherEvidence ?weather. ?weather o_lod:Cloudcover ?cloudCover. BIND(geof:distance(. . .) AS ?hazardDistance) BIND(o_lod:dem_value(. . .) AS ?objectElevation)	Binds cloud cover and the task-specific spatial and terrain relations.
Second	Constraint output	BIND(. . . AS ?themeQualified) BIND(. . . AS ?coverageQualified) BIND(. . . AS ?contextQualified)	Returns the values and separate condition outcomes used in the ablation runs.
	Full qualification	FILTER(?themeQualified && ?analysisQualified && ?timeQualified && ?coverageQualified && ?weatherQualified && ?contextObjectQualified)	Retains opportunities satisfying all four-dimensional task conditions.
	OCEM ranking	BIND(o_lod:ocem_planning_score(. . .) AS ?ocemScore) ORDER BY DESC(?ocemScore)	Calculates the priority score and orders all qualified opportunities.

The task-specific Context–Object clauses were implemented in the first layer. For Khartoum, they selected residential roads inside the 2 km Blue Nile corridor whose DEM-derived mean elevation was below the contextual average. For Bobcat, they evaluated the distance and terrain relation between Mount Wilson and the fire perimeter. The custom RDF4J function o_lod:dem_value() accepts a WGS 84 WKT geometry and returns the mean of the intersecting valid DEM cells. The second layer applied the OCEM-based evaluation through o_lod:ocem_planning_score(). Its inputs were the query-bound coverage, thematic conformity, cloud-cover effect, response timeliness, time coverage, revisit frequency, and spatial and spectral conformity. Across ten warm GraphDB executions, direct calls to o_lod:dem_value() and o_lod:ocem_planning_score() averaged 0.0043 ± 0.0014 s and 0.0056 ± 0.0016 s, respectively.

3.4.2. Constraint Contribution and Ranked Configuration Results

Table 6 summarizes the results obtained as the query conditions were applied successively. Satellite–sensor pairs and observation opportunities are reported separately because the theme, band, and resolution conditions are evaluated at the resource level, whereas space, time, daylight, context, and object conditions are evaluated for individual opportunities.

Table 6. Numbers of resources and opportunities returned by successive UDOT queries.

Entity Type	Configuration Stage	Khartoum	Bobcat
Satellite-sensor pair	Available resource pairs	202	202
	ObservationTheme parameter qualified	146	126
	Requested-analysis capable	3	4
Observation opportunity	TLE-predicted from analysis-capable pairs	5	15
	Event space/time and daylight qualified	2	8
	Context and Object qualified	2	8

Thematic matching retained most of the 202 available resource pairs in both cases, whereas the requested band and 30 m resolution requirements reduced them to three for Khartoum and four for Bobcat, which produced five and 15 opportunities within the respective task windows.

Table 7 reports opportunity-level leave-one-constraint-out results obtained by re-executing the first-layer query after removing one condition at a time. Each changed count is accompanied by a representative newly admitted opportunity and its query evidence. Theme and analysis capability are already quantified at the resource-pair level in Table 6 and are therefore not repeated in the opportunity-level ablation. The stricter Bobcat solar-elevation threshold was not binding beyond the daylight condition, since all seven opportunities admitted by its removal had negative solar elevation.

The complete query returned two qualified opportunities for Khartoum and eight for Bobcat. In Khartoum, Sentinel-2A/MSI on 9 September had predicted coverage of 99.8% and hourly cloud cover of 5%, while Landsat-7/ETM+ on 10 September had coverage of 100.0% and hourly cloud cover of 18%. Both opportunities covered the Blue Nile context and were associated with the 1153 residential roads satisfying the river-corridor and elevation conditions. The daylight Sentinel-2B/MSI opportunity on 7 September was excluded because its predicted coverage was only 0.7%.

Table 7. Planning-stage constraint contribution within the analysis-capable opportunity set (Arrows indicate the change in qualified-opportunity count from the ablated query to the full query; slash-separated values refer to Khartoum and Bobcat, respectively).

Case	Removed Constraint	Qualified Ablated → Full	Newly Admitted Resource	Bound Evidence or Role
Khartoum	Predicted AOI coverage ≥ 0.8	$3 \rightarrow 2$	Sentinel-2B/MSI, 7 Sep.	Predicted coverage was 0.66%; the opportunity could not support area-wide monitoring.
Khartoum	Solar elevation $> 0°$	$3 \rightarrow 2$	Sentinel-2B/MSI, 6 Sep.	Solar elevation was $-57.439°$, indicating a nighttime optical opportunity.
Bobcat	Predicted AOI coverage ≥ 0.8	$8 \rightarrow 8$	None	Every daylight opportunity already met the coverage threshold; the condition was not discriminative in this case.
Bobcat	Solar elevation $\geq 10°$	$15 \rightarrow 8$	Seven nighttime opportunities; e.g., Sentinel-2A/MSI, 6 Sep.	The example had a solar elevation of $-41.686°$.
Both	Cloud cover $\leq 50\%$	$2 \rightarrow 2/8 \rightarrow 8$	None	The retained opportunities met the threshold; cloud values remained relevant to OCEM environmental-impact scoring.
Both	Context–Object relation	$2 \rightarrow 2/8 \rightarrow 8$	None	The count was unchanged, but the query no longer established the link to low-lying riverside roads or the Mount Wilson target.

For Bobcat, the eight qualified opportunities were linked to Mount Wilson, which was 44.8 m from the historical fire perimeter and had an elevation of 1733 m compared with the contextual mean of 1365 m. Sentinel-2B/MSI on 10 September, for example, had predicted coverage of 83.3% and hourly cloud cover of 1%. The Sentinel-2A/MSI opportunity on 6 September was excluded because its solar elevation was below the specified threshold.

Under the main 30 m configuration, Sentinel-2A/MSI on 9 September ranked first for Khartoum with an OCEM score of 92.1, followed by Landsat-7/ETM+ on 10 September with 88.0. Sentinel-2A ranked higher despite the slightly greater coverage of Landsat-7 because it combined lower cloud cover with an earlier response. For Bobcat, Sentinel-2B/MSI on 10 September ranked first (112.9), followed by Landsat-7/ETM+ on 13 September (111.9) and Sentinel-2A/MSI on 15 September (109.9). The leading Sentinel-2B opportunity combined an early response, complete theme conformity, acceptable coverage, 1% cloud cover, and 10 m resolution.

The spatial-resolution requirement was varied to examine its effect on opportunity qualification and ranking. Relaxing the maximum acceptable resolution from 30 to 100 m, with all other conditions unchanged, increased the number of qualified Khartoum opportunities from two to six and reordered the ranking: Resourcesat-2A/AWiFS, IRS-P6/AWiFS,

and Resourcesat-2/AWiFS occupied the first three positions with OCEM scores of 98.6, 96.8, and 92.2, followed by Sentinel-2A/MSI, Landsat-7/ETM+, and a second IRS-P6/AWiFS opportunity. The resolution threshold therefore governs both the size and the ordering of the feasible set: a relaxed target-scale requirement admits wider-swath, moderate-resolution resources that score highly on coverage and revisit, whereas the 30 m configuration retains the alternatives suitable for object-level flood monitoring. The 100 m configuration is used in the following screenshots because it displays a broader set of ranked alternatives.

The query outputs could be inspected in O-LOD Viz, a visual query interface that combines a GraphDB-style binding table with a linked three-dimensional globe and switchable spatial layers. The same interface was used for both cases, and the Khartoum implementation is shown here. Figure 12 presents the first-layer diagnostic query: its result table retains the qualification state of each opportunity, while the globe displays the set of predicted satellite footprints and highlights the footprint associated with the selected qualified row. This view makes the spatial effect of the opportunity-level constraints directly inspectable alongside their RDF bindings.

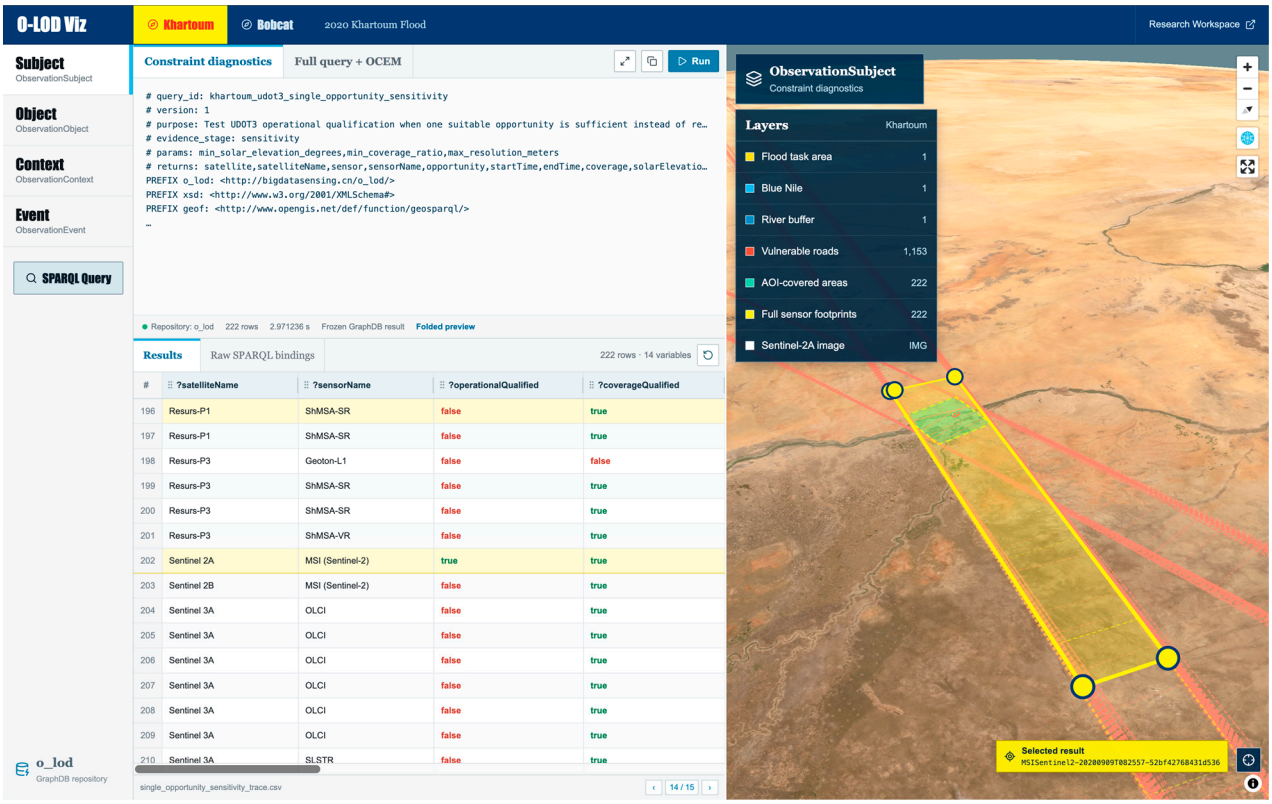


Figure 12. Opportunity-level constraint diagnostics for the Khartoum flood under the supplementary 100 m sensitivity configuration.

Figure 13 presents the full-query results in the OCEM-ranking mode of O-LOD Viz. The left panel preserves the descending OCEM order in a GraphDB-style result table, and the linked globe brings together the task AOI, Blue Nile and its buffer, vulnerable roads, qualified coverage areas, and the available Sentinel-2A image. Across ten warm executions, the complete Khartoum and Bobcat queries averaged 2.971 $\pm$ 0.018 s and 0.065 $\pm$ 0.001 s, respectively. The longer Khartoum execution reflects the terrain evaluation of 1153 road geometries, whereas the Bobcat query evaluates one declared target.

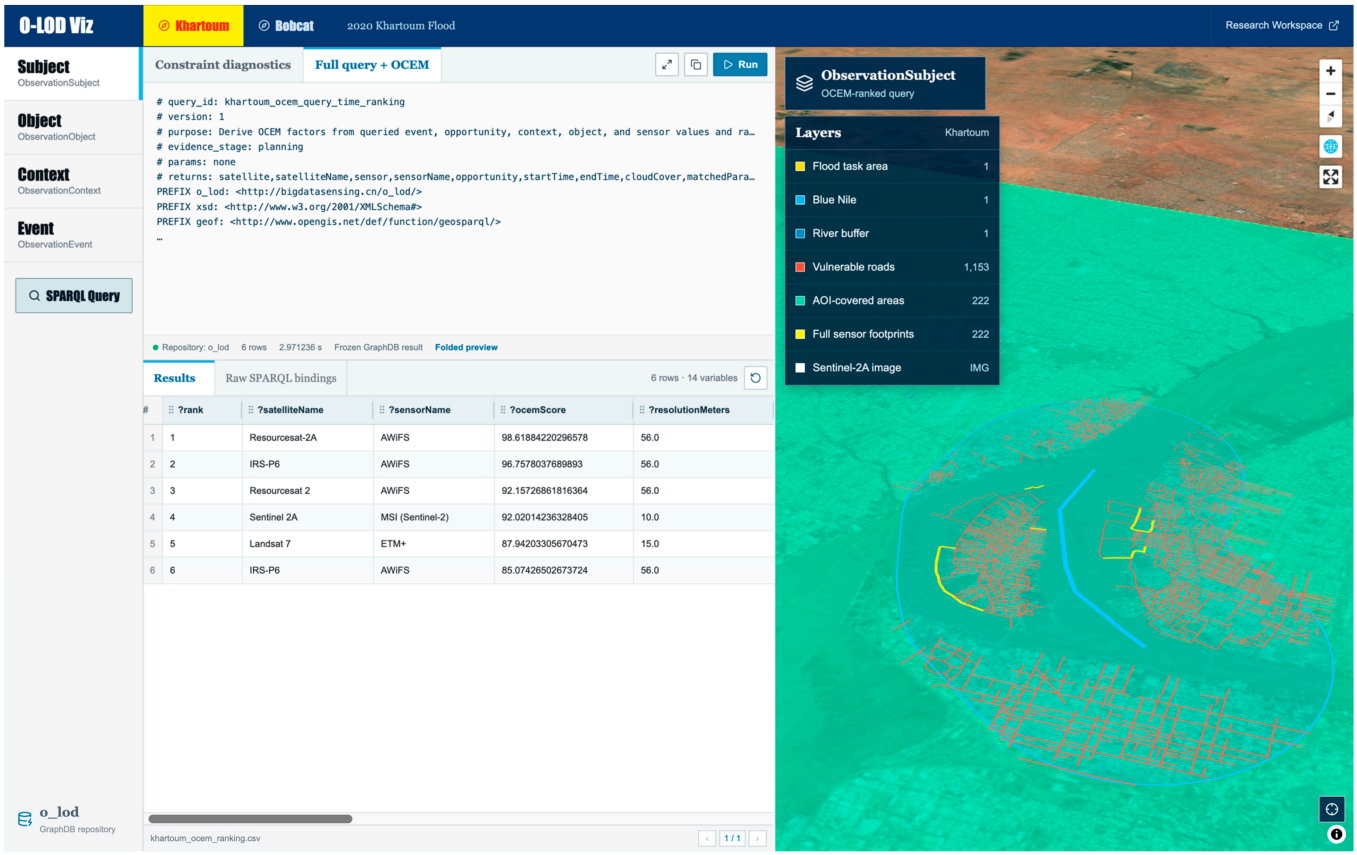


Figure 13. Full Khartoum UDOT query and OCEM-ranked results under the supplementary 100 m sensitivity configuration.

3.4.3. Validation with Publicly Accessible EO Products

Image validation was limited to products that could be obtained from publicly accessible EO archives (Table 8). For Khartoum, products were obtained for the two qualified opportunities and for one excluded Sentinel-2B opportunity used as a coverage comparison. For Bobcat, products were obtained for all eight qualified opportunities; an additional Terra/MODIS product was included to examine the effect of spatial resolution. Their actual footprints, scene cloud, required spectral bands, and usable pixels were compared with the task requirements, and suitable images were used for modified normalized difference water index (MNDWI) or differenced normalized burn ratio (dNBR) analysis.

In Khartoum, the rank-1 Sentinel-2A product supported an MNDWI comparison that identified a 14.2 km^2 new-water proxy (Figure 14). Six low-elevation road centerlines intersected this area, and 45 additional roads were within 60 m. By comparison, the Landsat-7 image covered the AOI but was obscured by cloud and cloud shadow, whereas the two Sentinel-2B tiles covered only 2.1–2.4% of the AOI. The three products therefore provided a usable flood-monitoring example and two distinct counterexamples for image quality and spatial coverage.

Table 8. Representative query results and evidence from publicly accessible EO products.

Case	Query Result	Public Product Evidence	Monitoring Assessment
Khartoum	Sentinel-2A/MSI, 9 Sep.; qualified, rank 1	Actual coverage 1.000; scene cloud 6.66%; readable Green and SWIR1 bands	The acquisition supports the flood-oriented MNDWI analysis
Khartoum	Landsat-7/ETM+, 10 Sep.; qualified, rank 2	Actual coverage 1.000, but scene cloud 81.00%; all valid AOI QA pixels were cloud or cloud shadow	Cloud and cloud shadow prevented flood-oriented MNDWI analysis
Khartoum	Sentinel-2B/MSI, 7 Sep.; excluded by predicted coverage	Predicted coverage 0.65%; two intersecting archive tiles covered only 0.020940–0.024149 of the AOI	The limited footprint was insufficient for area-wide flood monitoring
Bobcat	Sentinel-2B/MSI, 10 Sep.; qualified, rank 1	Actual coverage 1.000, but scene cloud 69.17%	High scene cloud prevented burn analysis.
Bobcat	Landsat-7/ETM+, 13 Sep.; qualified, rank 2	Actual coverage 1.000; scene cloud 2.00%; readable NIR and SWIR2 bands, but limited common-valid AOI pixels	Insufficient valid pixels around Mount Wilson prevented target-scale dNBR analysis
Bobcat	Sentinel-2B/MSI, 20 Sep.; qualified, rank 4	Actual coverage 1.000; scene cloud 0.05%; readable NIR and SWIR2 bands	The image was suitable for earlier post-fire NBR observation
Bobcat	Sentinel-2B/MSI, 30 Sep.; qualified, rank 8	Actual coverage 1.000; scene cloud 0.51%; readable NIR and SWIR2 bands	The image supported late-window NBR and dNBR analysis
Bobcat	Terra/MODIS; excluded by spatial resolution	The product covers the AOI and contains SWIR2, but its SWIR2 resolution is 500 m	The data cannot meet the 30 m requirement or resolve the 100 m target neighborhood

For Bobcat, five of the eight obtained products had sufficient coverage, spectral bands, and image quality for further examination; three were limited by acquired-image quality. The 13 September Landsat-7 image, for example, covered the AOI and reported 2% scene cloud, but only 13.6% of the AOI had common valid pre/post pixels, and none of the 35 pixels in the 100 m Mount Wilson neighborhood was common-valid, preventing target-scale dNBR analysis (Figure 15).

The 20 and 30 September Sentinel-2B products both provided full AOI coverage, the required NIR and SWIR2 bands, and low scene cloud. Pairing a 5 September pre-fire image with the 30 September image retained 99.6% common valid-pixel coverage and produced a mean dNBR of 0.289, including 7.8 km^2 of moderate and 3.6 km^2 of high change (Figure 16). Within 100 m of Mount Wilson, 68 of 77 pixel centers were valid; 56 indicated unburned or very low change and 12 indicated low change, with a mean dNBR of 0.041. The additional Terra/MODIS product covered the AOI and contained SWIR2, but its 500 m resolution could neither meet the 30 m requirement nor resolve the 100 m target neighborhood.

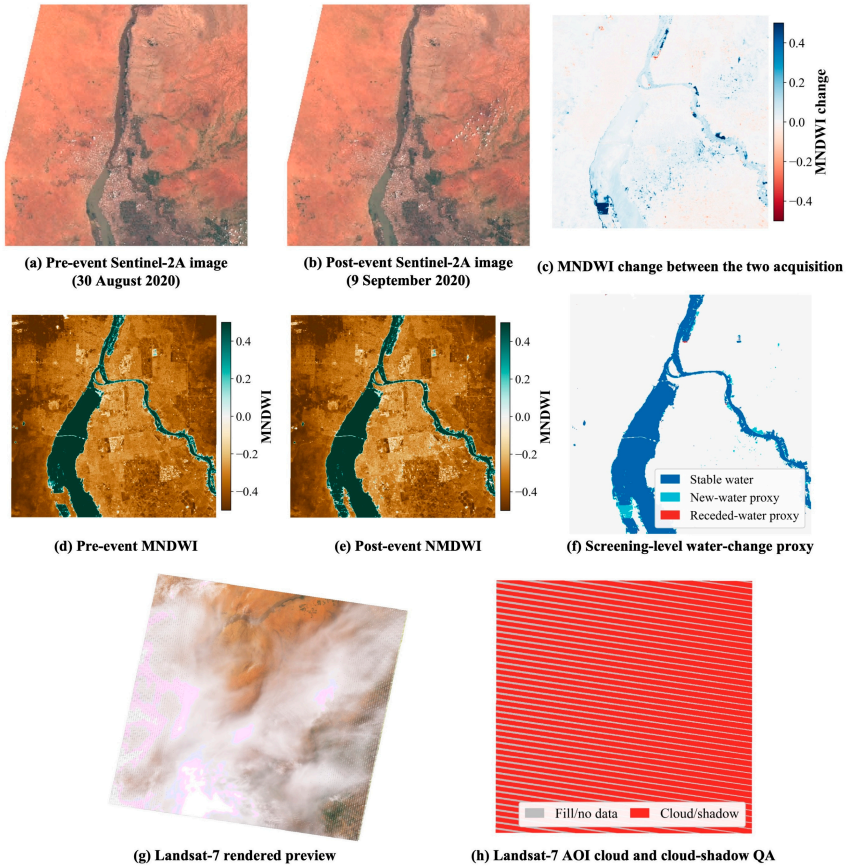


Figure 14. Khartoum archived-image evidence. MNDWI is used as a screening indicator rather than a field-validated flood-loss map.

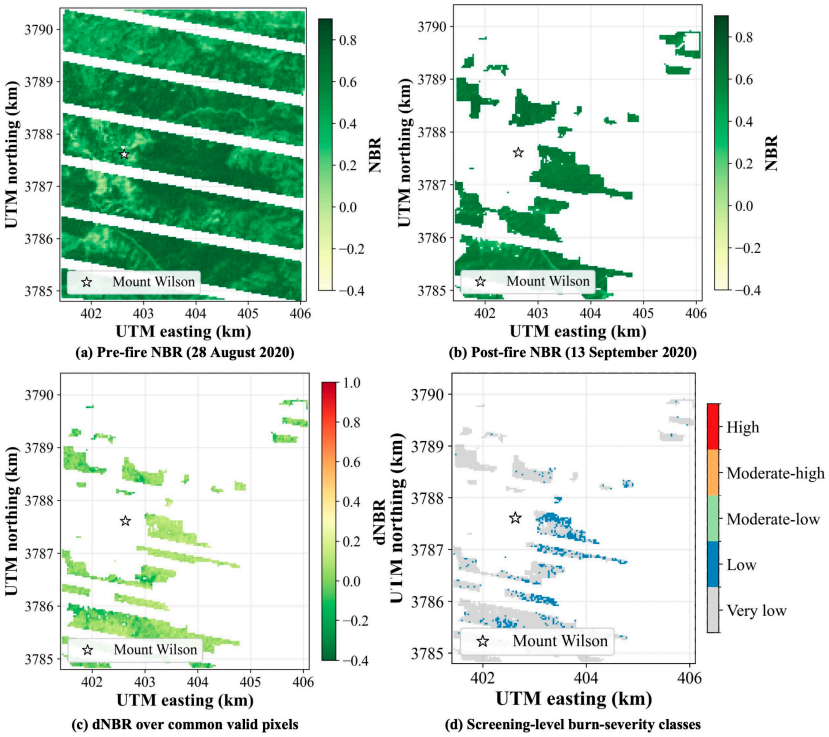


Figure 15. Image evidence from the 13 September Bobcat Landsat-7 product. White regions are invalid because of cloud, cloud shadow, fill, or SLC-off gaps; the star marks Mount Wilson.

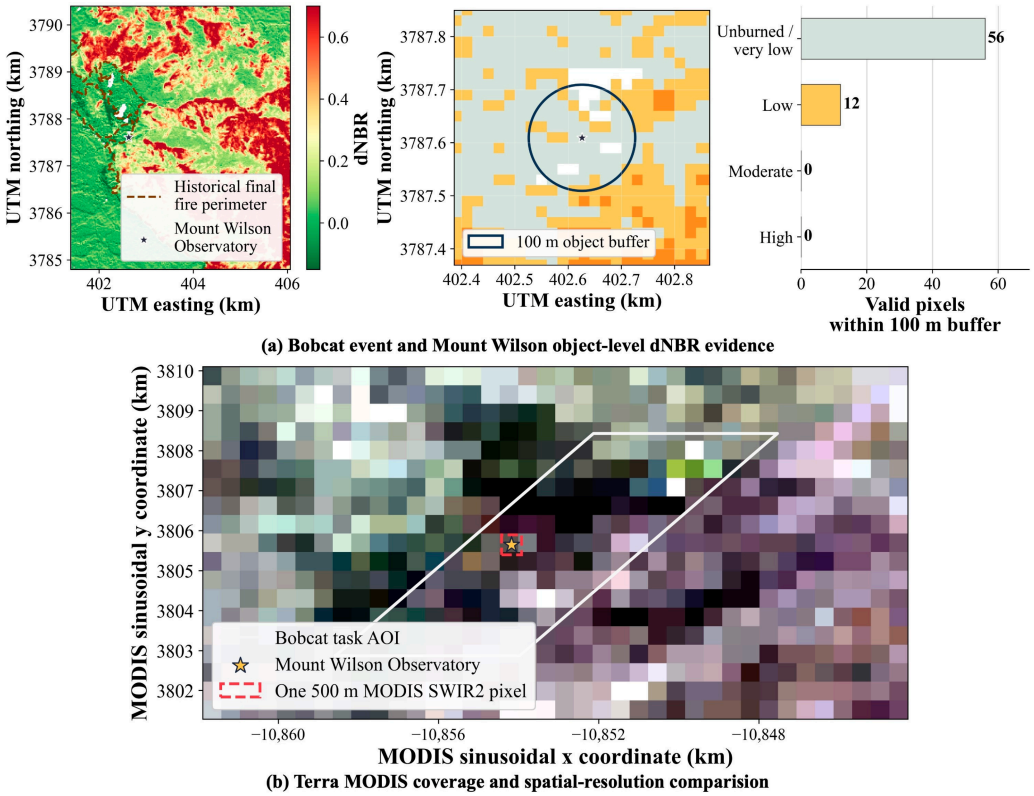


Figure 16. Bobcat image-analysis evidence at the event and target scales.

4. Discussion

4.1. Semantic Enhancement of EO Resource Planning for Urban Disaster Monitoring

The two experimental cases show that O-LOD supports EO resource planning as a progression from capability discovery to opportunity prioritization. Theme and analytical requirements first identify suitable satellite–sensor pairs; TLE-derived passes then provide time-specific observation opportunities; event, context, and object conditions determine task relevance; and OCEM orders the opportunities that satisfy the hard requirements. The complete queries retained two alternatives for Khartoum and eight for Bobcat. EO planning enabled by O-LOD therefore comprises the semantic discovery, qualification, and prioritization of EO opportunities, providing task-oriented inputs for subsequent satellite scheduling rather than solving the scheduling problem itself.

The results further demonstrate why the four dimensions must be evaluated together. In Khartoum, the flood theme and Green/SWIR1 requirement linked the monitoring demand to sensor capability, while the opportunity footprint, hourly cloud cover, Blue Nile corridor, terrain, and low-elevation roads established where and under what conditions the observation was relevant. In Bobcat, NIR/SWIR2 capability was evaluated together with the event window, fire perimeter, terrain, and the Mount Wilson target. The MODIS comparison is illustrative: the product intersected the wildfire area and contained SWIR2, but its 500 m SWIR2 resolution could not meet the 30 m requirement at the ObservationObject scale. Spatial intersection alone would therefore have returned a product that was not suitable for the stated task.

Publicly accessible products provided supporting evidence for both retained and excluded opportunities. The limited Sentinel-2B footprints in Khartoum were consistent with the predicted coverage exclusion, whereas the retained Sentinel-2A acquisition supported the flood-oriented MNDWI analysis. The cloud-obscured Khartoum Landsat-7 and Bobcat Sentinel-2B images show that a high planning rank cannot guarantee the quality

of a particular acquisition. Conversely, later Bobcat Sentinel-2B images provided usable NIR and SWIR2 data for NBR and dNBR analysis. Thus, opportunity ranking expresses suitability under the event and context evidence available to the query, while the subsequent image assessment determines whether an acquired product can support the intended analysis. Hourly cloud cover remains useful before acquisition, but it should be updated by image-derived quality evidence when a product becomes available.

The semantic contribution of the cross-dimensional constraints lies in the task-aware graph patterns that connect GeoSPARQL operations and numeric conditions with controlled observation semantics. ObservationParameter IRIs align event demand with sensor capability; platform, sensor, and opportunity ownership remain explicit; weather is joined to opportunity time; contextual features are related to urban objects; and qualification reasons, OCEM factors, acquisitions, and analysis provenance remain connected. The resulting evidence chain allows a query to return a resource together with the requirements it matched, the context and target evidence used, its relative rank, and the subsequent product assessment.

From a geospatial digital twin perspective, this evidence chain provides a task-oriented sensing layer between representations of urban state and the resources used to inspect and update them. The Bobcat graph further shows that the same ontology structure and instantiation process can be applied to a wildfire task without changing the four-dimensional query logic, supporting structural reuse across flood and wildfire monitoring tasks.

4.2. Comparative Analysis and Framework Extensibility

Table 9 compares representative approaches by their primary purpose, Event–Context–Object coupling, and role in a UDOT workflow. SSN/SOSA provide general sensor and observation semantics [31–33]; SOCA and the Sensor Observation Capability Field (SOCO-Field) focus on EO capability association and context-aware selection [18,34]; OFPO formalizes flood-process observation knowledge [36]; GEOSatDB organizes civil EO satellite metadata [39]; and operational catalogues provide authoritative resource or product access [20–23]. These approaches address complementary problems. O-LOD specifically composes event demand, time-indexed context, sensing opportunities, urban targets, qualification evidence, ranking, and archive provenance for UDOT configuration.

The functional comparison highlights the task-oriented semantic scope of O-LOD. By preserving these relations in one graph, it supports a traceable progression from disaster observation demand to qualified and ranked opportunities and subsequent image assessment.

Further development should focus on dynamic graph updating and scalable geospatial computation. The current cases use historical, time-stamped evidence, including hourly records retrieved from a public weather service, whereas operational flood and wildfire monitoring would require incremental weather, hazard-extent, and observation-opportunity updates. Higher-fidelity meteorological inputs, such as satellite-derived cloud masks or numerical forecasts, can be substituted through the same ObservationContext interface without modifying the qualification model, and versioned named graphs and stream ingestion provide a path toward windowed reasoning and continuous GeoSPARQL queries. At the present task scale, the complete Khartoum and Bobcat queries averaged 2.971 s and 0.065 s, respectively. The o_lod:dem_value() and o_lod:ocem_planning_score() functions expose DEM-derived terrain evidence and the capability score directly to GeoSPARQL, but both are RDF4J extensions rather than standard GeoSPARQL functions; reproducing these queries on another triple store therefore requires equivalent extensions or delegation of the corresponding computation to an external geospatial service. For larger or more frequently

updated graphs, RDF and GraphDB can retain semantic alignment, task configuration, and provenance, while repeated raster, geometry, and orbit calculations are delegated to PostGIS or equivalent geospatial services.

Table 9. Comparison of representative approaches by primary purpose, Event–Context–Object coupling, and role in the UDOT workflow.

Approach	Primary Purpose	Event-Context-Object Coupling	Task Role and Comparison Boundary
SSN/SOSA [31–33]	Generic sensors, observations, samples, and actuators	Not disaster-task specific	Reusable observation vocabulary; does not itself generate EO opportunities or a UDOT evidence chain
SOCA [34]	Dynamic and inherent EO sensing-capability association	Event, environment, and urban-target linkage is outside its main scope	Subject-capability specialization presented as an ontology model rather than a case-instantiated urban-disaster graph
SOCO-Field [18]	GeoTask-oriented capability and field/context constraints	Includes selected context such as cloud cover; limited target-object modeling	Supports context-aware sensor selection; not designed for the complete four-dimensional product/provenance chain evaluated here
OFPO [36]	Flood-process observation ontology and workflow	Rich flood-process semantics; hazard-domain specific	Supports flood observation knowledge organization; not a cross-hazard opportunity-ranking and archive-validation service
GEOSatDB [39]	Global civil EO satellite semantic database	Task event, dynamic environment, and urban objects are not its primary focus	Structured satellite metadata and discovery; complementary input to task-level configuration
CEOS, OSCAR, HDDS, GEE, and STAC [20–23,52]	Resource cataloguing or EO product access and processing	Platform-specific filters and product metadata rather than one task ontology	Authoritative metadata and data access; catalogues do not by themselves connect all four UDOT dimensions
O-LOD/UDOT	Disaster-driven semantic resource discovery and prioritization	Explicit Event, Context, Subject, and Object task patterns	Generates, qualifies, ranks, and traces opportunities and later products; does not solve spacecraft scheduling

The current ObservationObject conditions express task-specific exposure and relevance. They can be enriched with population exposure, structural condition, functional criticality, accessibility, land use, service dependencies, and multitemporal deformation, consistent with multivariate remote-sensing vulnerability assessment. OCEM can likewise incorporate additional factors such as incidence angle, commercial cost, licensing, downlink delay, and information gain when consistent data and stakeholder weights are available. This would extend the present opportunity ranking toward more comprehensive decision support.

The public-product evidence supports the reported case analyses, while a larger expert-labeled benchmark is required for independent estimates of selection precision and recall. MNDWI and dNBR can also be combined with field observations or authoritative impact records in future applications.

4.3. Implications for Sustainable Urban Resilience and the SDGs

The proposed framework has implications for sustainable urban resilience. First, O-LOD can support more resource-efficient EO configuration by narrowing data discovery and analysis to observations that meet the task requirements. The opportunity-level ablation showed that removing spatial-coverage or daylight constraints admitted observations that could not support the intended monitoring, and the public-image comparisons identified cloud-obscured or locally invalid products before thematic interpretation. Together, these mechanisms can reduce unsuitable opportunity selection and unnecessary downstream data processing.

Second, O-LOD improves the transparency of disaster observation planning by linking an opportunity to event demand, sensing capability, environmental context, target evidence, OCEM factors, the corresponding EO product, and analysis provenance. A user can inspect why an opportunity was qualified or ranked and whether the later image supported the intended monitoring. OSM and DBpedia references remain directly accessible through owl:sameAs, while public product identifiers make the image evidence traceable. This supports explainable and reproducible decision preparation for urban disaster response.

Third, the framework reuses open and linked resources while allowing local domain facts where specialized sensor or contextual information is required. The two cases integrate OSM, terrain data, historical TLEs, hourly weather, public sensor catalogues, and accessible Sentinel, Landsat, and MODIS products within a common task-oriented graph structure. This is relevant to data-scarce or budget-constrained regions because the semantic layer is not tied to a single proprietary platform. Private sensors, commercial constraints, and deep-learning-derived vulnerability products provide directions for extending this open-data foundation.

The sustainability contribution of O-LOD is primarily situated at the level of information infrastructure and disaster-oriented decision support. Interoperable EO resource planning and open-data integration support resilient infrastructure and innovation under Sustainable Development Goal (SDG) 9; target-oriented and traceable urban disaster evidence supports disaster-risk reduction and urban resilience under SDG 11; and context-aware flood and wildfire observation supports climate-hazard preparedness and adaptation under SDG 13 [1–5]. Achieving the corresponding SDG targets also depends on broader operational, institutional, and socioeconomic action.

5. Conclusions

This study developed an O-LOD-based UDOT enhancement framework for semantic EO resource planning in urban disaster monitoring. O-LOD represents ObservationEvent, ObservationContext, ObservationSubject, and ObservationObject within a unified RDF graph, and uses the O-LOD boundary model and O-LOD instantiation algorithm to transform heterogeneous open and domain data into task-oriented knowledge. Layered GeoSPARQL queries connect observation themes and analytical requirements with sensor capabilities, TLE-derived opportunities, time-specific weather, terrain, hazard-related spatial relations, and urban targets. Qualified opportunities are subsequently prioritized with OCEM, providing a traceable progression from observation demand to ranked EO resources and corresponding product evidence.

The Khartoum flood and Bobcat wildfire cases demonstrated the framework under different observation demands. From 202 satellite–sensor pairs in each case, capability matching identified three flood-oriented and four wildfire-oriented pairs; event, opportunity, context, and object constraints retained two Khartoum and eight Bobcat opportunities, which were ranked by OCEM. Coverage and daylight ablations admitted demonstrably unsuitable opportunities, while publicly accessible products supplied external supporting

evidence at the image level. Sentinel and Landsat data supported MNDWI and NBR/dNBR analyses when coverage, spectral bands, and usable pixels met the task requirements; limited footprint, cloud contamination, or coarse MODIS resolution explained other exclusions or unusable acquisitions. The complete queries averaged 2.971 s for Khartoum and 0.065 s for Bobcat. These results show that O-LOD can combine semantic resource discovery, target-specific context, opportunity ranking, and subsequent image assessment within one queryable evidence chain. Through open-data integration and explicit provenance, this evidence chain provides information and decision support for resource-aware and transparent urban disaster monitoring

Future work will extend the framework in three directions. First, dynamic event and context updates will be incorporated through versioned graph states, stream ingestion, and richer causal and relational structures informed by event knowledge graph research [54]. Second, intelligent query support will be explored through remote-sensing knowledge graphs, large language model (LLM)-assisted semantic retrieval, and natural-language-to-GeoSPARQL translation [55,56]. Third, ObservationObject modeling will be enriched with multivariate vulnerability indicators, while additional public and private EO sensors, in situ observations, and volunteered or social sensing data will extend O-LOD toward a broader cyber–physical–social observation framework [57,58].

Author Contributions: Conceptualization, J.L. and K.W.; methodology, J.L. and L.Z.; software, B.J., W.J. and X.D.; validation, J.L. and B.J.; formal analysis, J.L. and L.Z.; investigation, J.L. and W.J.; resources, L.Z. and X.D.; data curation, B.J., W.J. and X.D.; writing—original draft preparation, J.L.; writing—review and editing, K.W.; visualization, B.J. and X.D.; supervision, K.W.; project administration, L.Z. and K.W.; funding acquisition, J.L., L.Z., W.J. and K.W. All authors have read and agreed to the published version of the manuscript.

Funding: This research was supported by grants from the National Key R&D Program of China under Grant No. 2024YFC3811003, by the National Natural Science Foundation of China (NSFC) under Grant Nos. 42401508 and 42471517, by the China Postdoctoral Science Foundation under Grant No. 2024M763064, by the Commissioned project of the Technology Innovation Center for Ecological Protection and Restoration Engineering in the Middle Reaches of the Yellow River, Ministry of Natural Resources under Grant No. HHZY-2025-014, by the Ministry-Province Cooperation Project of the Ministry of Natural Resources under Grant No. 2024ZRBSHZ003, and by the Wuhan Municipal Science and Technology Bureau Scientific and Technological Achievement Transformation Project under Grant No. 2023030103010726.

Institutional Review Board Statement: Not applicable.

Informed Consent Statement: Not applicable.

Data Availability Statement: The data presented in this study are available in Figshare at https://figshare.com/s/896a2a5cc8b222f4f78c (accessed on 16 August 2026).

Conflicts of Interest: Author Wu Jing was employed by Wuhan Hanyang Municipal Construction Group Co., Ltd. The remaining authors declare that the research was conducted in the absence of any commercial or financial relationships that could be construed as a potential conflict of interest.

References

1. Dodman, D.; Hayward, B.; Pelling, M.; Castan Broto, V.; Chow, W.; Chu, E.; Dawson, R.; Khirfan, L.; McPhearson, T.; Prakash, A.; et al. Cities, Settlements and Key Infrastructure. In *Climate Change 2022: Impacts, Adaptation and Vulnerability. Contribution of Working Group II to the Sixth Assessment Report of the Intergovernmental Panel on Climate Change*; Pörtner, H.O., Roberts, D.C., Tignor, M., Poloczanska, E.S., Mintenbeck, K., Alegría, A., Craig, M., Langsdorf, S., Löschke, S., Möller, V., et al., Eds.; Cambridge University Press: Cambridge, UK; New York, NY, USA, 2022; pp. 907–1040. ISBN 978-1-009-32584-4.
2. Dharmarathne, G.; Waduge, A.O.; Bogahawaththa, M.; Rathnayake, U.; Meddage, D.P.P. Adapting Cities to the Surge: A Comprehensive Review of Climate-Induced Urban Flooding. *Results Eng.* **2024**, *22*, 102123. [CrossRef]

3. Akinsanola, A.A.; Singhai, P.; Taguela, T.N.; Folorunsho, A.H.; Adeyeri, O.E.; Morakinyo, T.E.; Adebiyi, A.A. A Review of Urban Resilience to Weather and Climate Extremes. *City Built Enviro* **2025**, *3*, 24. [CrossRef]
4. Menoni, S. Urban Planning for Disaster Risk Reduction and Climate Change Adaptation: A Review at the Crossroads of Research and Practice. *Sustainability* **2025**, *17*, 9092. [CrossRef]
5. Disaster Risk and the 2030 Agenda for Sustainable Development | UNDRR. Available online: https://www.undrr.org/implementing-sendai-framework/drr-focus-areas/disaster-risk-and-2030-agenda-sustainable-development (accessed on 9 July 2026).
6. Bacher, U. Hybrid Aerial Sensor Data as Basis for a Geospatial Digital Twin. *Int. Arch. Photogramm. Remote Sens. Spat. Inf. Sci.* **2022**, *XLIII-B4-2022*, 653–659. [CrossRef]
7. Ranatunga, S.; Ødegård, R.S.; Onstein, E.; Jetlund, K. Digital Twins for Geospatial Decision-Making. *ISPRS Ann. Photogramm. Remote Sens. Spat. Inf. Sci.* **2024**, *X-4–2024*, 271–278. [CrossRef]
8. Therias, A.; Rafiee, A. City Digital Twins for Urban Resilience. *Int. J. Digit. Earth* **2023**, *16*, 4164–4190. [CrossRef]
9. Ham, Y.; Kim, J. Participatory Sensing and Digital Twin City: Updating Virtual City Models for Enhanced Risk-Informed Decision-Making. *J. Manag. Eng.* **2020**, *36*, 04020005. [CrossRef]
10. Rolla, J.; Khuller, A.; An, K.; Emberson, R.; Fielding, E.; Schultz, L.; Miner, K.R. Satellite-Aided Disaster Response. *AGU Adv.* **2025**, *6*, e2024AV001395. [CrossRef]
11. Chen, H.; Peng, S.; Du, C.; Li, J. *Earth Observation Satellites: Task Planning and Scheduling*; Springer: Singapore, 2023; ISBN 978-981-99-3564-2.
12. Zhang, Y.; Li, J.; Duan, M.; Chen, W.; del Rio, J.; Zhang, X.; Wang, K.; Liang, S.H.L.; Chen, Z.; Chen, N.; et al. Multi-Sensor Integration Management in the Earth Observation Sensor Web: State-of-the-Art and Research Challenges. *Int. J. Appl. Earth Obs. Geoinf.* **2023**, *125*, 103601. [CrossRef]
13. Peuquet, D.J.; Duan, N. An Event-Based Spatiotemporal Data Model (ESTDM) for Temporal Analysis of Geographical Data. *Int. J. Geogr. Inf. Syst.* **1995**, *9*, 7–24. [CrossRef]
14. Peng, S.; Chen, H.; Du, C.; Li, J.; Jing, N. Onboard Observation Task Planning for an Autonomous Earth Observation Satellite Using Long Short-Term Memory. *IEEE Access* **2018**, *6*, 65118–65129. [CrossRef]
15. Zhao, Z.; Hu, C.; Wang, K.; Zhang, Y.; Xu, Z.; Ding, X. An Earth Observation Task Representation Model Supporting Dynamic Demand for Flood Disaster Monitoring and Management. *Remote Sens.* **2023**, *15*, 2193. [CrossRef]
16. Jirka, S.; Bröring, A.; Stasch, C. Discovery Mechanisms for the Sensor Web. *Sensors* **2009**, *9*, 2661–2681. [CrossRef] [PubMed]
17. Zhang, X.; Chen, N.; Chen, Z.; Wu, L.; Li, X.; Zhang, L.; Di, L.; Gong, J.; Li, D. Geospatial Sensor Web: A Cyber-Physical Infrastructure for Geoscience Research and Application. *Earth-Sci. Rev.* **2018**, *185*, 684–703. [CrossRef]
18. Hu, C.; Li, J.; Xiao, C.; Wang, K.; Chen, N. SOCO-Field: Observation Capability Representation for GeoTask-Oriented Multi-Sensor Planning Cognition. *Int. J. Geogr. Inf. Sci.* **2020**, *34*, 205–228. [CrossRef]
19. Li, D.; Wang, M.; Xiao, J.; Yang, B. Perspectives on Spatio-Temporal Intelligence. *ISPRS J. Photogramm. Remote Sens.* **2026**, *232*, 305–318. [CrossRef]
20. CEOS | Committee on Earth Observation Satellites. Available online: https://ceos.org/ (accessed on 3 July 2026).
21. WMO OSCAR | Observing Systems Capability Analysis and Review Tool—Home. Available online: https://space.oscar.wmo.int/ (accessed on 3 July 2026).
22. Velastegui-Montoya, A.; Montalván-Burbano, N.; Carrión-Mero, P.; Rivera-Torres, H.; Sadeck, L.; Adami, M. Google Earth Engine: A Global Analysis and Future Trends. *Remote Sens.* **2023**, *15*, 3675. [CrossRef]
23. Hazards Data Distribution System (HDDS) | U.S. Geological Survey. Available online: https://www.usgs.gov/emergency-operations-portal/hazards-data-distribution-system-hdds (accessed on 24 March 2026).
24. Long, Y.; Shan, C.; Shang, W.; Li, J.; Wang, Y. Deep Reinforcement Learning-Based Approach with Varying-Scale Generalization for the Earth Observation Satellite Scheduling Problem Considering Resource Consumptions and Supplements. *IEEE Trans. Aerosp. Electron. Syst.* **2024**, *60*, 2572–2585. [CrossRef]
25. Zhou, G.; Jin, Z.; Liu, D. Deep Reinforcement Learning-Based Two-Phase Hybrid Optimization for Scheduling Agile Earth Observation Satellites. *Remote Sens.* **2025**, *17*, 1972. [CrossRef]
26. Li, C.; Tan, X.; Chen, C. Deep Reinforcement Learning–Driven Multi-Satellite Collaborative Observation Planning for Emergency and Disaster Monitoring. *Int. J. Digit. Earth* **2025**, *18*, 2554310. [CrossRef]
27. Wang, X.; Chen, N.; Chen, Z.; Yang, X.; Li, J. Earth Observation Metadata Ontology Model for Spatiotemporal-Spectral Semantic-Enhanced Satellite Observation Discovery: A Case Study of Soil Moisture Monitoring. *GISci. Remote Sens.* **2016**, *53*, 22–44. [CrossRef]
28. Hu, C.; Tian, L.; Li, J.; Wang, K.; Chen, N. An Observation Capability Information Association Model for Multisensor Observation Integration Management: A Flood Observation Use Case in the Yangtze River Basin. *IEEE Sens. J.* **2019**, *19*, 11510–11525. [CrossRef]
29. Kumari, S.; Agarwal, S.; Agrawal, N.; Agarwal, A.; Garg, M. A Comprehensive Review of Remote Sensing Technologies for Improved Geological Disaster Management. *Geol. J.* **2024**, *60*, 223–235. [CrossRef]

30. Compton, M.; Barnaghi, P.; Bermudez, L.; García-Castro, R.; Corcho, O.; Cox, S.; Graybeal, J.; Hauswirth, M.; Henson, C.; Herzog, A.; et al. The SSN Ontology of the W3C Semantic Sensor Network Incubator Group. *J. Web Semant.* **2012**, *17*, 25–32. [CrossRef]
31. Janowicz, K.; Haller, A.; Cox, S.J.D.; Le Phuoc, D.; Lefrançois, M. SOSA: A Lightweight Ontology for Sensors, Observations, Samples, and Actuators. *J. Web Semant.* **2019**, *56*, 1–10. [CrossRef]
32. Semantic Sensor Network Ontology—2023 Edition. Available online: https://www.w3.org/TR/vocab-ssn-2023/ (accessed on 3 July 2026).
33. Hu, C.; Li, J.; Lin, X.; Chen, N.; Yang, C. An Observation Capability Semantic-Associated Approach to the Selection of Remote Sensing Satellite Sensors: A Case Study of Flood Observations in the Jinsha River Basin. *Sensors* **2018**, *18*, 1649. [CrossRef] [PubMed]
34. Li, J.; Hu, C.; Yi, X.; Wang, K.; Chen, N. OCAGraph: An Effective Observation Capability Association Model for Earth Observation Sensor Planning. *Int. J. Appl. Earth Obs. Geoinf.* **2022**, *114*, 103038. [CrossRef]
35. Du, W.; Liu, C.; Xia, Q.; Wen, M.; Hu, Y.; Chen, Z.; Xu, L.; Zhang, X.; Terfa, B.K.; Chen, N. OFPO & KGFPO: Ontology and Knowledge Graph for Flood Process Observation. *Environ. Model. Softw.* **2025**, *185*, 106317. [CrossRef]
36. Wang, C.; Zhuo, X.; Li, P.; Chen, N.; Wang, W.; Chen, Z. An Ontology-Based Framework for Integrating Remote Sensing Imagery, Image Products, and In Situ Observations. *J. Sens.* **2020**, *2020*, 6912820. [CrossRef]
37. Zhang, Y.; Chen, W.; Huang, B.; Zhang, Z.; Li, J.; Gao, R.; Wang, K.; Hu, C. An Event Logic Graph for Geographic Environment Observation Planning in Disaster Chain Monitoring. *Int. J. Appl. Earth Obs. Geoinf.* **2024**, *134*, 104220. [CrossRef]
38. Lin, M.; Jin, M.; Li, J.; Bai, Y. GEOSatDB: Global Civil Earth Observation Satellite Semantic Database. *Big Earth Data* **2024**, *8*, 522–539. [CrossRef]
39. Chen, M.; Cao, X. Construction of Remote Sensing Early Warning Knowledge Graph Based on Multi-Source Disaster Data. *Remote Sens.* **2025**, *17*, 3594. [CrossRef]
40. Berners-lee, T. Linked Data—Design Issues. Available online: https://www.w3.org/DesignIssues/LinkedData.html (accessed on 3 July 2026).
41. Shimizu, C.; Stephen, S.; Barua, A.; Cai, L.; Christou, A.; Currier, K.; Dalal, A.; Fisher, C.K.; Hitzler, P.; Janowicz, K.; et al. The KnowWhereGraph Ontology. *J. Web Semant.* **2025**, *84*, 100842. [CrossRef]
42. Li, W.; Wang, S.; Chen, X.; Tian, Y.; Gu, Z.; Lopez-Carr, A.; Schroeder, A.; Currier, K.; Schildhauer, M.; Zhu, R. GeoGraphVis: A Knowledge Graph and Geovisualization Empowered Cyberinfrastructure to Support Disaster Response and Humanitarian Aid. *ISPRS Int. J. Geo-Inf.* **2023**, *12*, 112. [CrossRef]
43. Car, N.J.; Homburg, T. GeoSPARQL 1.1: Motivations, Details and Applications of the Decadal Update to the Most Important Geospatial LOD Standard. *ISPRS Int. J. Geo-Inf.* **2022**, *11*, 117. [CrossRef]
44. Hu, Y.; Janowicz, K.; Prasad, S.; Gao, S. Enabling Semantic Search and Knowledge Discovery for ArcGIS Online: A Linked-Data-Driven Approach. In *AGILE 2015: Geographic Information Science as an Enabler of Smarter Cities and Communities*; Springer: Berlin/Heidelberg, Germany, 2015; pp. 107–124. ISBN 978-3-319-16786-2.
45. Mai, G.; Janowicz, K.; Yan, B.; Scheider, S. Deeply Integrating Linked Data with Geographic Information Systems. *Trans. GIS* **2019**, *23*, 579–600. [CrossRef]
46. Kopsachilis, V.; Vaitis, M. GeoLOD: A Spatial Linked Data Catalog and Recommender. *Big Data Cogn. Comput.* **2021**, *5*, 17. [CrossRef]
47. Gangemi, A.; Mika, P. Understanding the Semantic Web through Descriptions and Situations. In *On The Move to Meaningful Internet Systems 2003: CoopIS, DOA, and ODBASE*; Meersman, R., Tari, Z., Schmidt, D.C., Eds.; Lecture Notes in Computer Science; Springer: Berlin/Heidelberg, Germany, 2003; Volume 2888, pp. 689–706. ISBN 978-3-540-20498-5.
48. Duan, M.; Zhang, Y.; Liu, R.; Chen, S.; Deng, G.; Yi, X.; Li, J.; Yang, P. Observation Capability Evaluation Model for Flood-Observation-Oriented Satellite Sensor Selection. *Appl. Sci.* **2023**, *13*, 12482. [CrossRef]
49. Rodríguez Antuñano, I. Vulnerability Assessment of Urban Infrastructure from Remote Sensing Data Using Advanced Analysis Techniques. Ph.D. Thesis, Universidade de Vigo, Vigo, Spain, 2024. [CrossRef]
50. Rodríguez-Antuñano, I.; Riveiro, B.; Martínez-Sánchez, J.; Soilán, M. Large-scale monitoring of terrestrial infrastructure to anticipate extreme events using SAR interferometry. In Proceedings of the 10th International Conference on Structural Health Monitoring of Intelligent Infrastructure (SHMII-10), Porto, Portugal, 30 June–2 July 2021; pp. 1445–1450.
51. Janowicz, K.; Hitzler, P.; Adams, B.; Kolas, D.; Vardeman, C. Five Stars of Linked Data Vocabulary Use. *Semant. Web* **2014**, *5*, 173–176. [CrossRef]
52. *OGC Document 25-004*; SpatioTemporal Asset Catalog (STAC) Community Standard, Version 1.1. Open Geospatial Consortium: Arlington, VA, USA, 2025. Available online: https://docs.ogc.org/cs/25-004/25-004.html (accessed on 6 August 2026).
53. Ontotext. GraphDB Downloads and Resources. Available online: https://graphdb.ontotext.com/ (accessed on 3 July 2026).
54. Guan, S.; Cheng, X.; Bai, L.; Zhang, F.; Li, Z.; Zeng, Y.; Jin, X.; Guo, J. What Is Event Knowledge Graph: A Survey. *IEEE Trans. Knowl. Data Eng.* **2023**, *35*, 7569–7589. [CrossRef]

55. Zhu, Q.; Jia, Q.; Xie, W.; Liu, C.; Shen, T.; Zhang, Z.; Wang, W. Construction of Remote Sensing Knowledge Graph for Spatiotemporal Analysis. *IEEE J. Sel. Top. Appl. Earth Obs. Remote Sens.* **2026**, *19*, 7341–7356. [CrossRef]
56. Wei, Y.; Zhang, C.; Yue, P.; Li, H. Geospatial Knowledge Cube: Enhancing Semantic Query in Geospatial Data Cubes with Ontology and LLMs. *Int. J. Geogr. Inf. Sci.* **2026**, 1–32. [CrossRef]
57. Yin, W.; Deuser, F.; Liu, Z.; Wei, J.; Luo, X.; Werner, M.; Li, H.; Xue, Y. Triple-Objective Cross-View Geolocalization of Disaster-Related VGI: The Case of Hurricane Ian. *Int. J. Geogr. Inf. Sci.* **2026**, *40*, 194–216. [CrossRef]
58. Pasandideh, S.; Pereira, P.; Gomes, L. Cyber-Physical-Social Systems: Taxonomy, Challenges, and Opportunities. *IEEE Access* **2022**, *10*, 42404–42419. [CrossRef]

Disclaimer/Publisher's Note: The statements, opinions and data contained in all publications are solely those of the individual author(s) and contributor(s) and not of MDPI and/or the editor(s). MDPI and/or the editor(s) disclaim responsibility for any injury to people or property resulting from any ideas, methods, instructions or products referred to in the content.